NTNU
Norwegian University of
Science and Technology

On the Stability of the Local Load Sharing Fiber Bundle Model

Eivind Bering

Master of Science in Physics and Mathematics
Submission date: June 2016
Supervisor: Alex Hansen, IFY

Norwegian University of Science and Technology
Department of Physics

“*To those who do not know mathematics it is difficult to get across a real feeling as to the beauty, the deepest beauty, of nature. . . . If you want to learn about nature, to appreciate nature, it is necessary to understand the language that she speaks in.*”

– Richard Feynman, *The Character of Physical Law* (1965).

Summary

This thesis investigates a generalized history-independent local load sharing (LLS) fiber bundle model for two dimensional interfacial fractures. When the failure threshold of the fibers are assigned according to the cumulative distribution

$$P(x) = 1 - e^{-x+x_0},$$

the model displays two distinct regimes separated by a critical transition. For systems with low cutoff x_0, the damage is developing through random weakening of the system, which resembles the equal load sharing (ELS) model. As the cutoff is increased, the behaviour approaches invasion percolation. This localization transition is determined to occur at the critical cutoff

$$x_c = 0.6173 \pm 0.0005,$$

with a critical exponent

$$\beta/\nu = 1.5 \pm 0.1.$$

The LLS model displays a local stability not seen in the ELS model. By estimating the cutoffs that results in the highest positive slope in the strain curve for a range of lattice sizes, extrapolation to the thermodynamic limit reveals a cutoff that coincides with the critical cutoff, with a correlation length exponent

$$\nu = 2.$$

This stability originates in the short-range interaction of the model, which effectively stresses the strong fibers the most. Moreover, the LLS model is shown to be globally more stable than the ELS model when $x_0 \lesssim 0.5$. The global stability of the LLS model vanishes around the critical transition. This is related to a change in the distribution of bursts, i.e. the fibers that fails consecutively. For the LLS model, the burst distribution is shown to be consistent with a power law $D(\Delta) \sim \Delta^{-\tau}$, with burst exponent

$$\tau = 2$$

around the critical transition. Analog to the criticality of the ELS model at $x_0 = 1$, lower cutoffs results in higher burst exponents, and cutoffs above x_c gives rise to exponential decay in the burst distribution. The distribution of fatal bursts, which cause the entire bundle to rapture, reveals a drastic change of behaviour around the critical transition. For cutoffs above x_c, far fewer fibers may break before the bundle would undergo catastrophic failure in a force controlled experiment.

Sammendrag

Denne masteravhandlingen omhandler en generalisert historieuavhengig fiberbundt-modell med lokal lastdeling (LLS) i to dimensjoner. Når fibrenes bruddstyrke er tatt fra den kumulative fordelingen

$$P(x) = 1 - e^{-x+x_0},$$

viser modellen to ulike regimer. For systemer med lav avkutting x_0 sprer skaden i systemet seg tilfeldig, og oppførselen ligner det en ser i modellen for lik lastdeling (ELS). Med økende avkutting nærmer oppførselen til systemet seg det en finner med invasjonsperkolasjon. Denne lokaliseringsovergangen finner sted ved den kritiske avkuttingen

$$x_c = 0.6173 \pm 0.0005,$$

med en kritiske eksponent

$$\beta/\nu = 1.5 \pm 0.1.$$

LLS-modellen viser en stabilitet som ikke sees i ELS-modellen. Ved å estimere avkuttingen som resulterer i det høyeste stigningstallet i stresskurven for en rekke gitterstørrelser, gav ekstrapolering til den termodynamiske grensen en avkutting som sammenfaller med x_c, samt en korrelasjonslengdeeksponent

$$\nu = 2.$$

Denne stabiliteten skyldes den korte interaksjonsrekkevidden i modellen, som effektivt fordeler et høyere stress på de sterke fibrene. Videre er LLS-modellen vist å være globalt mer stabil enn ELS-modellen for $x_0 \lesssim 0.5$. LLS-modellen mister global stabilitet etter den kritiske overgangen. Dette er forbundet med en endring i fordelingen av etterfølgende brukne fibre. For LLS-modellen er denne fordelingen vist å være konsekvent med en potenslov $D(\Delta) \sim \Delta^{-\tau}$ med eksponent

$$\tau = 2$$

rundt den kritiske avkuttingen. Analogt til den kritiske oppførselen for modellen med lik lastdeling ved $x_0 = 1$, gir lavere avkuttinger en høyere eksponent τ, og for avkuttinger over x_c avtar $D(\Delta)$ eksponensielt. Fordelingen av etterfølgende brukne fibre som fører til total kollaps av fiberbundten avdekker en drastisk endring i oppførsel rundt den kritiske overgangen. For avkuttinger over x_c vil vesentlig færre fibre ryke før fiberbundten står i overhengende fare for å kollapse fullstendig i et eksperiment der kraften er den styrende parameteren.

Preface

The results presented in this thesis originates from work done during the last year of my Master of Technology degree in applied physics at The Norwegian University of Science and Technology (NTNU). The assignment is based on results found by Jonas Kjellstadli (2015) in his master thesis.

When people ask me what I do, my response is that I study damage propagation in materials, which is almost true. However, as fractures are rather complicated processes, we need models. The model I have been working on is called the local load sharing fiber bundle model, and it describes the force redistribution in an idealized fiber bundle under extension by an external force. It has surprised me how rich such a simple model may be, in terms of the range of disciplines it incorporates, and moreover, how well numerical results may be described mathematically. I have enjoyed working with this topic, and I hope the reader also find this text to be of some interest regardless of background and prior knowledge concerning the fiber bundle model.

I would like to thank my supervisor Alex Hansen for his thorough follow-up and motivating feedback. The recent book on the topic of fiber bundle models by Hansen *et al.* (2015) was truly inspiring, and made the the field of fiber bundle modelling accessible to a much larger extent. I would also like to thank the Departement of Physics at NTNU for providing me access to the computer cluster, which has been indispensable for my simulations. I would also like to thank postdoctoral researcher Santanu Sinha for his aid in the early stages of this assignment.

The process of scientific work may at times be demanding. When unanswered questions pile up, and the computer program is infected with numerous bugs, some assistance might do all the difference. I would express my sincere gratitude to Jonas T. Kjellstadli for his great insight and thorough answers regarding the various phenomenas displayed by the fiber bundle model. Moreover, I owe a debt of gratitude to Morten Vassvik which guided me through his technique of graphical programming, and taught me a great deal concerning coding in general. The simulation program made during this semester would not have been half as good without his guidance. Håkon T. Nygård, Jørgen Vågan and Magnus H-S Dahle has made a great team. Their continuous support and motivation was of great value.

Table of Contents

List of Figures

Nomenclature

β	Order parameter exponent
Δ	Burst size
Δ_c	Crossover in the burst distribution
Δ_{fatal}	A fatal burst, that cause the entire bundle to rapture
κ	Hookean spring constant
ν	Correlation length exponent
ψ	Order parameter for the localization
σ	Stress, i.e. force per fiber
τ	Power law exponent for the burst distribution
ξ	Correlation length
F	External force on the system
h	Number of broken fibers in a cluster
k	Number of broken fibers in the bundle
k_{max}	Time step at which the strain curve has a maximum
L	System size
N	Total number of fibers in the system, $N = L^2$
n_c	Total number of clusters

$P(\Delta_{fatal})$ Cumulative probability for a fatal burst to occur

p_c Percolation transition

s Number of intact fibers along the perimeter of a cluster

x Extension of the fiber bundle

x_0 Cutoff in the probability distribution $P(x) = 1 - e^{-x+x_0}$

x_c Critical cutoff in the thermodynamical limit

x_f Critical cutoff in a finite sized system

x_i Failure threshold of fiber i

Chapter 1

Introduction

One of the most important tasks in engineering is to forsee, prevent and understand material failure. In the spirit of Hansen *et al.* (2015), let us first appreciate that theories such as *linear* and *non-linear elastic fracture mechanics* have unquestionably been very successful in describing material failure from a top-down approach, cf. Lawn (1993). Furthermore, atomistic modeling is also advancing rapidly, cf. Buehler (2008). However, as these models are highly computationally demanding for complex structures, cf. Gjerden (2013), fiber bundle models may in some applications prove to be a more viable alternative. As formulated by Hansen *et al.* (2015), fiber bundle models *"simplify the problems to the point where the very powerful methods of theoretical physics, statistics and mathematics may be fully explored"*. Could the fiber bundle models even reveal some general characteristics for fracture-failures?

In the context of this model, a *fiber* is understood as a spring obeying Hooks' law in one dimension until a critical extension has been reached, at which the fiber breaks and is no longer carrying a force. A fiber bundle consists of multiple fibers connected between two clamps. When a fiber breaks, the clamps may deform, depending on the model, as elaborated in Chapter 2. In the *local load sharing* (LLS) model this deformation is uniquely defined given the broken fibers in a bundle, as the model is *history independent*, as emphasized by Sinha *et al.* (2015). One does not need to know the order at which each fiber breaks to determine the stress distribution in the bundle.

The LLS model is in many aspects a simple model. Considering the dictum often accredited to William of Ockham, known as Ockham's razor: *"Plurality must never be posited without necessity"* Franklin (2001), this is advantageous compared to other models. Comparable to how the Ising model captures some of the complex behaviour of magnetic materials with a set of simplistic rules, the LLS

model may describe important aspects of fractures in fibrous materials by only a few basic governing equations.

Most materials are not fibrous, but then again, most materials are not continuous either. With a basis in the fiber bundle model one may study phenomena like strain hardening, creep failure and fatigue failure in a wide range of materials, and the model could even be applied to analyze snow avalanches and landslides, as discussed in Hansen *et al.* (2015). This paper however, will mainly focus on investigation of results presented by Sinha *et al.* (2015).

When Jonas Kiellstadli was working on his master thesis (2015), he made the curious discovery that in the LLS model, where the load of the fibers is not equally distributed, there is a stability not found in the model where the force is equally distributed amongst all the fibers, i.e. the *equal load sharing* (ELS) model.

> *"Hence, stress-enhancement at the edges of holes leads to more stability than the lack of such. Very curious indeed!"*
>
> – Hansen *et al.* (2015).

In physics, nothing is more interesting than curiosities that seems to contradict common sense. From where does this increased stability originate? What is the driving mechanism? Is this simply an artifact of the model, or does it have any physical applications? This stability was investigated in the project thesis by Bering (2016), of which this thesis is a continued development.

Deeper understanding of this stability was considered to be the major goal of this Master's thesis. In the project assignment it was linked to a critical transition known as *localization*. This transition was identified and described, and one of the critical exponents was found. However, the need for better statistics was of great significance. This was solved by writing a faster simulation program.

Another goal of this work was to gain deeper understanding of the localization transition. Dahle (2016) introduced an order parameter for the localization, and found a value for the critical cutoff $x_c = 0.61 \pm 0.02$ with a respective critical exponent $\beta/\nu = 1.5 \pm 0.1$. By studying this order parameter further, the critical cutoff was determined with higher accuracy.

The study of *bursts*, i.e. consecutive failures, was devoted special attention. Pradhan *et al.* (2006) and Petri *et al.* (1994) emphasize that when *fracture-failures* in composite materials is studied experimentally, these failure avalanches typically represent the only measurable quantity. Thus, the burst distribution may allow for connections between the computer generated simulations and force controlled experiments. A change in behaviour of the burst distribution may signal imminent catastrophic failure of materials, hence this is a topic of great general interest.

This thesis is organized as follows: First the various fiber bundle models is outlined in Chapter 2, together with some theory regarding percolation, critical

phase transitions and finite size scaling. The essential computational methods is then outlined in Chapter 3, before the results is presented in Chapter 4. The results are then discussed and interpreted in Chapter 5. Following this, conclusions is drawn in Chapter 6, together with some directions for further research. Finally, the appendix contains a draft to an article that will be submitted to Physical Review upon completion.

Chapter 2

The Fiber Bundle Models

The fiber bundle model was first introduced by Peirce (1926) to model strength of textiles, in a form now recognized as the equal load sharing fiber bundle model. In this model all the fibers in the bundle experience the same force. This may be illustrated as a bundle of fibers stretched between two infinitely stiff clamps, as in Figure 2.1a. Under these conditions one may describe the behaviour of the fiber bundle in great detail analytically, and the reader is strongly encouraged to study the recent book by Hansen *et al.* (2015), where the fiber bundle models are discussed extensively.

When the clamps are not infinitely behaviour, deformations in the clamps occur each time a fiber breaks. For the sake of simplicity, one may assume that one clamp is infinitely behaviour, as this gives rise to the same physical behaviour, cf. Hansen *et al.* (2015). In the soft clamp model illustrated in Figure 2.1b, the other clamp is assigned a finite elasitic constant, so that the force on the intact fibers depends on the elastic response of the soft clamp, Sinha *et al.* (2015). Intact fibers adjacent to broken fibers now experience an increased load, and the next fiber to break is determined by the ratio of stress to failure threshold of the fiber. The implication of this is that fibers may break either due to having a low failure threshold or due to being highly stressed.

In the soft clamp model, the deformations of the clamps may be calculated by a set of Green functions, as conducted by Gjerden (2013) and Stormo (2013). This model is highly complex both mathematically and computationally. The local load sharing model introduced by Harlow and Phoenix (1978) represents a major simplification of the soft clamp model that may serve as a preferable alternative for many applications as it appear to capture important aspects of the soft clamp model at a fraction of the computational cost.

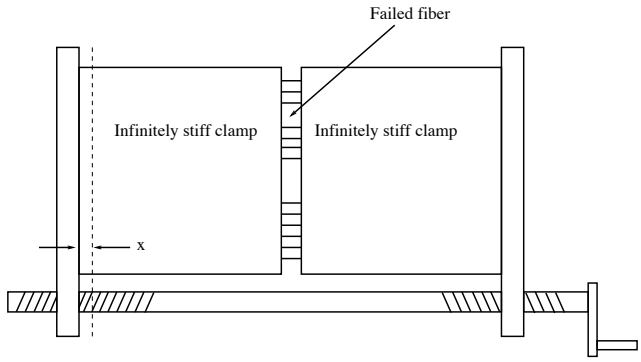

(a) The equal load sharing fiber bundle model.

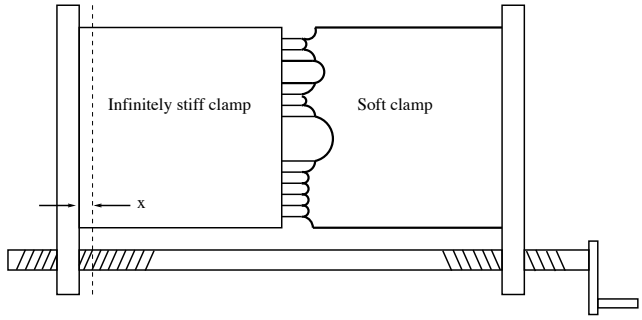

(b) The soft clamp fiber bundle model.

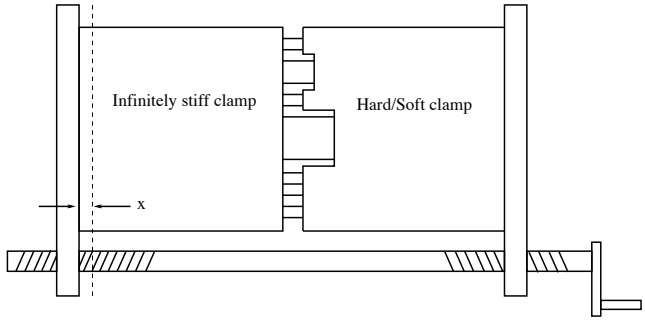

(c) The local load sharing fiber bundle model.

Figure 2.1: *Illustration of various fiber bundle models*, from Hansen *et al.* (2015). Note the definition of x, representing the extension of the fiber bundle without deformations.

2.1 Force redistribution rule

In the LLS model all the load of the broken fibers is distributed evenly among the nearest intact fibers, such that the force on the bundle remains $F = \kappa N x$ when one or more fibers break, where x is defined as the distance between the clamps without deformation, as illustrated in Figure 2.1c. The average force per fiber is then

$$\sigma = \frac{F}{N} = \kappa x \tag{2.1}$$

at all times. In one dimension this rule for redistribution of forces summarizes to

$$\sigma_i = \kappa\Big[1 + \frac{1}{2}(h_l + h_r)\Big]x, \tag{2.2}$$

where h_l and h_r is the number of broken fibers adjacent to the intact fiber counting to the left and right respectively. The broken fibers form *clusters* or holes, i.e. collections of broken fibers in direct connection with each other. The load of the broken fibers is evenly distributed between the two intact fibers adjacent to the cluster, as illustrated in Figure 2.1c. In two dimensions, the geometry of the clusters is more complex. The load of the cluster is evenly distributed among the intact fibers along the perimeter of the of the cluster, i.e. all the nearest intact fibers. Accordingly, the force redistribution rule reads

$$\sigma_i = \kappa\Big[1 + \sum_j \frac{h_j}{s_j}\Big]x, \tag{2.3}$$

where the summation is over all the clusters of broken fibers that are nearest neighbour to fiber i. Further, h_j denotes the number of broken fibers in the neighbouring cluster j, and s_j denotes the intact fibers in the perimeter of the corresponding cluster.

2.2 Breaking criteria

To determine which fiber will break next, we apply *quasistatic loading*. After a fiber breaks, the extension of the fiber bundle is reduced to zero, and then increased until another fiber breaks. With this approach only one fiber breaks for each time step. The first fiber to break will be the one that first reaches

$$\sigma_i = \kappa x = \kappa x_i. \tag{2.4}$$

Here x_i is the failure threshold of the fiber, and x is the extension of the bundle. With the observation $\sigma_i(x = 1) = \sigma(1) = \kappa$, a general breaking rule may be

expressed as

$$\max_i \left(\frac{\sigma_i(1)}{x_i} \right) = \frac{\kappa}{x} \tag{2.5}$$

which is applicable for all the subsequent breaking fibers. We note that this is the inverse of the extension at which a fiber breaks. The quantity $x_i/\sigma_i(1)$ will be referred to as the *effective threshold*. As the model assumes the fibers behave as Hookean springs until they break, this rule is valid also for $x < 1$. In the following, the spring constant κ is set equal to one. The LLS model is completely defined by the force redistribution rule from Equation (2.3) and the breaking rule from Equation (2.5), cf. Hansen *et al.* (2015). Note that with $\kappa = 1$, the stress and the strain of the fiber bundle model is the same quantity. The curve for the stress is typically denoted as the *strain curve*.

2.3 Strain curve

The strength of the fibers are assigned from a statistical distribution, and hence there will be fluctuations around the average values. These fluctuations are essential for the breakdown process in the fiber bundle model, and for studying fractures in materials in general. First it is useful to study some average properties. In the ELS model the average force per fiber in a strain-controlled experiment will simply be

$$\sigma(x) = x[1 - P(x)], \tag{2.6}$$

as $N(1-P(x))$ fibers are expected to have a failure threshold above x. Hence, the strain curve $\sigma = \sigma(k/N)$ may be derived by order statistics as shown by Hansen *et al.* (2015), to obtain the least force per fiber required to break the next fiber. In the simulations presented here, the failure thresholds of the fibers are distributed according to the exponential distribution with cutoff x_0, with the cumulative distribution function

$$P(x) = 1 - e^{-x+x_0}, \quad x \in [x_0, \infty). \tag{2.7}$$

This is the continuous equivalent of the geometric distribution, and is the only memoryless random distribution there is[1]. In the ELS model, this gives a force-elongation curve as seen in Figure 2.2. The corresponding strain curve is given by the expression

$$\sigma = \kappa \left(1 - \frac{k}{N}\right) \left(x_0 - \log\left(1 - \frac{k}{N}\right)\right), \tag{2.8}$$

[1] http://mathworld.wolfram.com/ExponentialDistribution.html

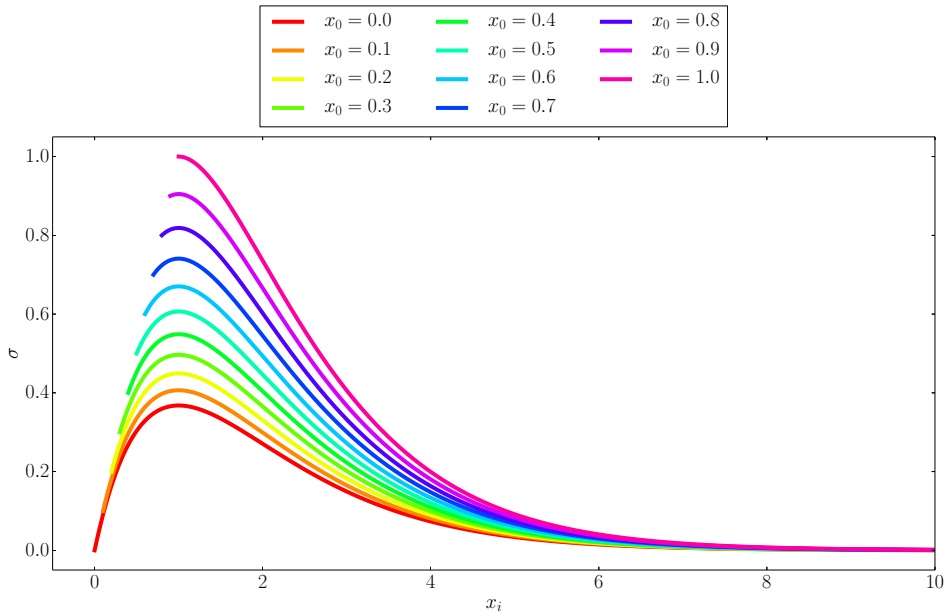

Figure 2.2: *Force against bundle elongation for the ELS model:* The strain on the bundle is shown as a function of the extension of the fiber that breaks for various cutoffs $x_0 \in [0, 1]$ in the exponential probability distribution for the failure thresholds of the fibers.

and is shown in Figure 2.3 for various cutoffs x_0 in the probability distribution. The strain curve for the LLS model follows directly from the breaking criteria in Equation (2.5).

2.4 Bursts

To compare these quasistatic strain controlled simulations with force controlled experiments it might be useful to study the avalanches of fibers that fails simultaneously. A *burst* of size Δ is defined to occure when Δ fibers break consecutively which all require a lower force to break than the force initiating the burst[2]. The distribution of bursts $D(\Delta)$ is studied as the bundle is loaded until breakdown. This distribution typically follows a power law

$$D(\Delta) \sim \Delta^{-\tau}, \tag{2.9}$$

[2]This is called an exclusive burst, as opposed to an inclusive burst which which only counts the fibers that break with a lower effective threshold than the previous fiber. The latter was not investigated in this thesis.

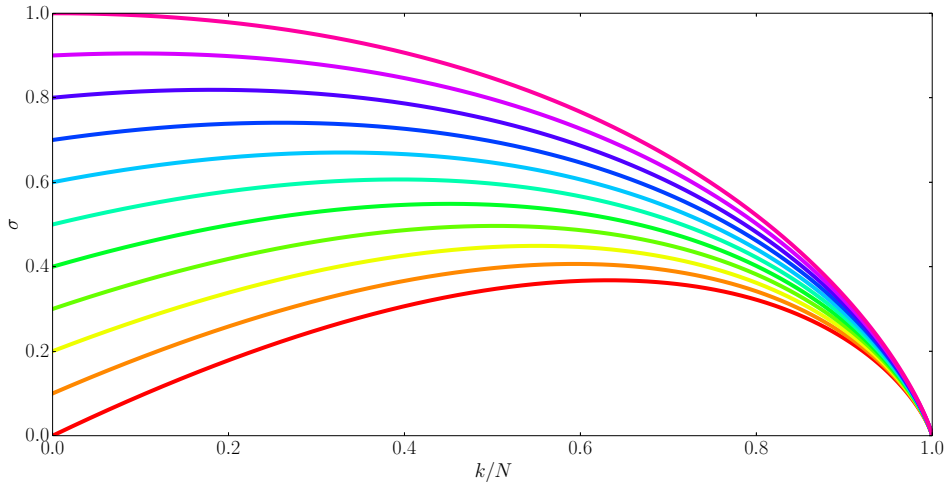

Figure 2.3: *Strain curve for the ELS model* for various cutoffs $x_0 \in [0, 1]$. Legend as in Figure 2.2.

and Hemmer and Hansen (1992) found that the burst distribution for the ELS model follows a universal asymptotic power law with $\tau = 5/2$ for large bursts. This is independent of the threshold distribution of the fibers; the only criteria is that the average macroscopic force $\langle F(x) \rangle$ has a single parabolic maximum, and that the systems are sufficiently large. Note that with the probability distribution from Equation (2.7), the corresponding strain curve shown in Figure 2.3 does not have a parabolic maximum for $x_0 \geq 1$. The burst exponent τ may change near complete breakdown. For the ELS model, bursts near the strain curve maximum follow a power law with $\tau = 3/2$. This indicates a loss of stability. Pradhan *et al.* (2006) describes the crossover from $\tau = 3/2$ to $\tau = 5/2$ in great detail. For the threshold distribution from Equation (2.7), the shift in burst exponent occur for bursts of size

$$\Delta_c = \frac{2}{(1 - x_0)^2}. \tag{2.10}$$

By sampling the burst distribution within a finite window, the $3/2$ power law will occur when the interval is close to the breaking point. A crossover in the burst exponent is typically strongly related to the catastrophic failure of the material.

2.5 Critical phase transitions

The theory of critical phase transitions and finite size scaling is used interdisciplinary. The critical temperature in the Ising model is a famous example of such

a transition, solved analytically by Onsager (1944). The following brief theory regarding percolation, critical exponents and finite size scaling originates from Stauffer and Aharony (1993) and Stanley (1987), which the interested reader is highly recommended to read.

2.5.1 Percolation

When the fibers that break are nearest neighbours to other broken fibers, they form clusters. The evolution of such clusters on a lattice is described generally by *percolation theory*. In percolation theory one usually considers the occupation probability p, and in terms of the fiber bundle this corresponds to the density of broken fibers k/N. All percolation systems undergo a *percolation transition* when the system has a finite non-zero probability of containing a *spanning cluster* of occupied sites, connecting the top and the bottom of the lattice so that an infinite network would occur if the lattice had been infinitely large.

2.5.2 Critical exponents

Critical phase transitions of second order or higher may in general be described by critical exponents, cf. Stanley (1987). From this, the properties of the transitioning system may be approximated by a power law behaviour. Close to the critical points, there is a single length scale that determines the range of interaction, as emphasized by Stauffer and Aharony (1993). This is the correlation length, denoted by ξ. Let p_c be the percolation threshold. Near the critical point the correlation length behaves like

$$\xi \sim |p - p_c|^{-\nu}, \tag{2.11}$$

such that ξ diverges when p approaches p_c. Here ν is the *correlation length exponent*, and for percolation this is one of the universal exponents. They are valid for all percolating systems described by the same percolation model. Another universal exponent is the *order parameter exponent* β, defined by the relation

$$\psi \sim |p - p_c|^{\beta} \tag{2.12}$$

where ψ is the *order parameter*. These are parameters that are characteristic for the transitioning system, and the order parameter is typically zero ahead of the critical point and nonzero after. The percolation transition is described by multiple order parameter. One is the *percolation strength*, defined as the fraction of occupied sites belonging to the largest cluster in the system, and another is the *mean cluster size*. Order parameters is used in a wide range of fields to describe critical behaviour. One example is the critical phase transition in the Ising model, where the magnetization is the order parameter.

Close to the transition, the universal exponents obey the *hyperscaling relation*

$$d - 2 + \eta = 2\beta/\nu, \tag{2.13}$$

where d is the dimensionality and η represents a correction to the scaling dimension, and goes by the name *anomalous dimension*. This however, is not a major topic of this text.

2.5.3 Finite size scaling

All numerical simulations on a finite size lattice is subject to finite size effects. The field of finite size scaling theory was introduced by Fisher and Barber (1972). Quantities obtained from lattices of finite length need to be extrapolated to determine the behaviour in the thermodynamic limit. The scaling laws from Subsection 2.5.2 are not only valid for the occupation probability. One may be interested in other quantities related to the particular transition phenomena. Let the quantity of interest be denoted by q. Introduce the notation q_f for the critical value of this parameter for a finite sized lattice, and let the critical value for an infinitely large lattice be denoted by q_c. For a system of finite size L, the correlation length is equal to the system length sufficiently close to the critical transition. The effective critical threshold q_f then relates to the asymptotic value q_c as

$$q_f - q_c \propto L^{-1/\nu} \tag{2.14}$$

such that ν and q_c may be found by calculating

$$q_f = q_c + C_1 L^{-1/\nu} \tag{2.15}$$

for various trial values of ν. One then selects the value for ν which gives the best straight line for large system sizes. If a corresponding order parameter ψ is found for the critical transition, this will scale like

$$\psi \propto L^{-\beta/\nu} \tag{2.16}$$

very close to the critical point, cf. Stanley (1987). This originates from the postulate of ξ being the only length scale of interest. When two of the critical exponents are known, e.g. ν and β, all other critical exponents follow by the hyperscaling relation.

2.5.4 Localization

In the LLS fiber bundle model, fibers that are nearest neighbours to clusters of broken fibers experience an increased load. Moreover, as the load of the broken

fibers in the cluster is evenly distributed at the perimeter, at some point all the fibers that break will be located along the perimeter of the largest cluster. Thus the fiber in the perimeter of the hole with the the lowest threshold is broken in each time step. In the LLS fiber bundle model a single growing cluster defines the onset of *localization*. This breaking process is identical to the *invasion percolation* model with nearest neighbour interaction, a model originating from the study of drainage in porous media, see e.g. Hansen *et al.* (2015). The localization transition should not be confused with the former mentioned percolation transition.

As suggested by Dahle (2016) a suitable order parameter associated with the localization transition in the LLS fiber bundle model is the average of the inverse of the highest number of separate clusters that occur during the failure process

$$\psi = \left\langle \frac{1}{\max_k\{n_c(k)\}} \right\rangle, \tag{2.17}$$

where n_c is the total number of clusters in the system.

Chapter 3

Computation

This chapter presents some of the central algorithms used and a few specifics regarding the simulations. As mentioned in Chapter 1, the need for better statistics was of great significance. This was solved by writing a faster program. This allowed for highly improved statistics. The most essential aspects of this program is the force redistribution and the breaking criteria, and hence this is outlined in Subsection 3.1.1. Moreover, Subsection 3.1.2 gives a short description of how the information is stored during the simulation.

3.1 Algorithms and simulations

The main concept is to follow the intact fibers along the perimeters of the clusters of broken fibers. As opposed to the conventional methods of following the broken fibers, this limits the computational effort considerably. The complete bundle state is known for all time steps, and only the minimal necessary updates is done throughout the simulation. The main program is written in C++ and utilizes the xorshift1024* random number generator[1] which has a period of about 2^{1024}, more than sufficient for these simulations. The seed of each simulation was stored to allow for reproducibility of the data. Numerous programs was written in Python to produce plots, and a Python program handles organization and merging of simulation files. All computationally demanding calculations was run on the computer cluster at the Departement of Physics at NTNU. At `www.daim.idi.ntnu.no`, the main simulation program is uploaded together with this paper.

[1] Documentation: `http://xorshift.di.unimi.it/`

3.1.1 Finding the fiber with lowest effective threshold

The intact fibers are divided in three categories:

- Fibers that are not nearest neighbour to any broken fibers
- Fibers that are included at least one perimeter
- Fibers included in at least one additional perimeter

By sorting all the fibers by the threshold, the first mentioned category is trivial. The intact fibers that is neighbouring broken fibers is organized by sorting the fibers in each perimeter by the failure threshold of the fibers. Furthermore, by sorting the perimeters by the effective threshold of the weakest fibers in each perimeter, the fiber with the highest effective threshold is easily accessible. With this structure, only a handful of updates is necessary for each time step. However, the fibers included in multiple perimeters requires to be studied separately. When a fiber breaks, all the fibers in the growing perimeter included in more than one perimeter must be revised. This constitute the dominant bottle neck in the program. However, as explained below, by switching the data structures for these fibers during the simulation the running time is reduced.

3.1.2 Data structures

Each perimeter is structured as a AVL tree, with fiber threshold as key. AVL trees (Georgy Adelson-Velsky and Evgenii Landis' tree) are self balancing binary search trees which guarantees insertion and deletion to scale as $\log(N)$, see e.g. Mehlhorn and Sanders (1999). All the perimeters are structured in another AVL tree, where the key is the effective threshold of the weakest fibers in each perimeter. Finally, all the fibers included in more than one perimeter are sorted by effective threshold in a separate data structure. Moreover, each perimeter is associated with a linked list of fibers that are included in both this perimeter and at least one additional perimeter. This allows for updating only the necessary fibers in multiple perimeters.

In the beginning of the breaking process, the fibers in multiple perimeters are also stored in an AVL tree. However, the updates necessary for each time step increase as more fibers break and the perimeters increase. At some point it becomes more effective to store all the fibers in multiple perimeters in a vector. This vector is not sorted, which demands all the elements to be evaluated for each time step. Figure 3.1 display how the running time for the simulation program is varying with cutoff and the time step k/N at which the fibers in multiple perimeters is stored in vectors instead of AVL trees.

However, the standard associative container `std::set` in C++ might be a better alternative. This is implemented as red-black trees, which has faster deletion and insertion, at the cost of slower look-up, cf. Cormen *et al.* (2001).

The web page `http://kukuruku.co/hub/cpp/avl-trees` was very helpful in the understanding of AVL trees, and the AVL data structure was implemented with a basis in this. The web page was written by Nikolai Ershov at the Russian Academy of Sciences in 2008.

3.2 Visualization

Application of the OpenGL[2] library GLFW[3] allowed for real time visualization of the bundle state during the simulations, which also eased the debugging. Figure 3.2 displays how the state of the bundle could be visualized during the simulation. Black squares indicate broken fibers, and the fibers along the perimeter of each cluster is marked with colored circles. Although barely visible in this Figure, fibers in multiple perimeters is marked with a green dot. Figure 3.3 and Figure 3.4 display the visualization of the AVL data structures with GLFW, where the colors are similar to the respective perimeters seen in Figure 3.2.

[2] An open source cross-language programming interface for developing high-efficiency cross-platform graphics applications. Documentation: `https://www.opengl.org`

[3] Documentation: `www.glfw.org/`

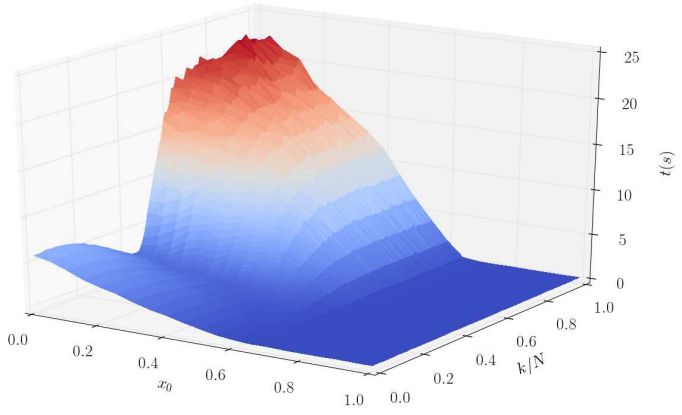

Figure 3.1: *Running time* in seconds as a function of cutoff x_0 and the time step k/N at which the data structure for the fibers in many perimeters is changed.

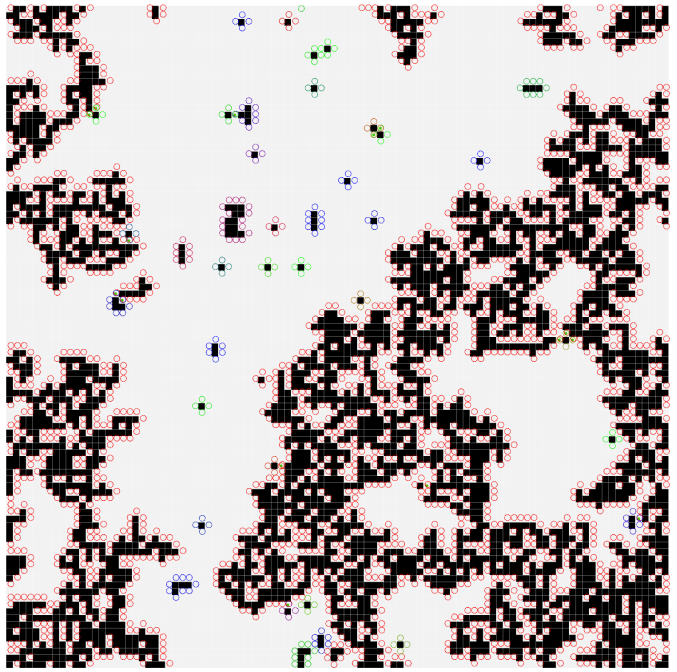

Figure 3.2: *Bundle state with perimeters* as visualized with GLFW.

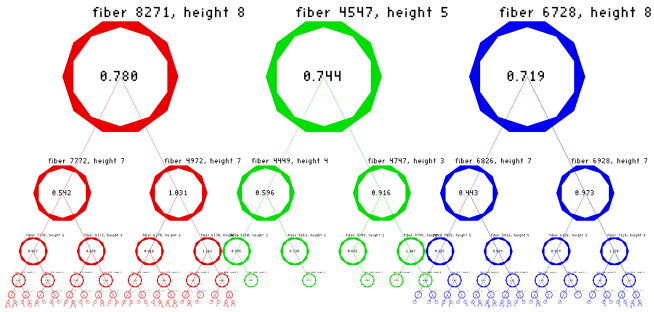

Figure 3.3: *The AVL trees of the perimeters* as visualized with GLFW.

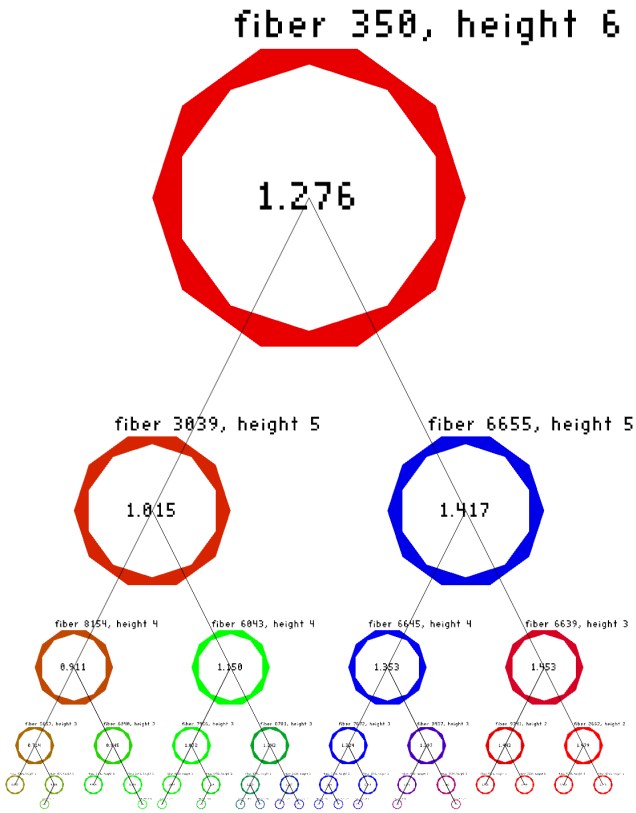

Figure 3.4: *AVL tree for the fibers in many perimeters* as visualized with GLFW.

Chapter 4

Results

This chapter presents the results from simulations of the ELS and LLS model described in Chapter 2. When the failure thresholds of the fibers are distributed according to the cumulative exponential distribution $P(x) = 1 - e^{-x+x_0}$ with cutoff x_0, the LLS model is shown to undergo a phase transition at some *critical cutoff* x_c. Systems of various sizes have been studied to account for finite size effects. First, Section 4.1 is meant to give a qualitative understanding of the behaviour of the model during this transition, before the transition is investigated qualitatively by means of the order parameter ψ from Equation (2.17). After this, the strain curve and the associated stability mentioned in Chapter 1 is studied in Section 4.3. As for the burst distribution, this is first studied for the ELS model in Section 4.4. With a basis in this, the burst distribution was then investigated for the LLS model in Section 4.5.

4.1 Two phases

The damage spreading in the LLS model for various cutoffs can be seen in Figure 4.1, where the system state is visualized at time step $k/N = 0.2$. The systems with cutoffs $x_0 = 0$ and $x_0 = 1$ yields an disordered and an ordered phase respectively, and the model appear to change behaviour around $x_0 = 0.617$. In Figure 4.2 the system state is shown at $k/N = 0.58$. The difference is less obvious, however still noticeable. In the figure for $x_0 = 0$ there are 801 perimeters, and 4554 fibers are in more than one perimeter. For $x_0 = 0.617$, there are 40 perimeters, and 70 fibers are in more than one perimeter. In the figure shown for $x_0 = 1$ all the broken fibers belong to the same cluster. This suggests that the two phases may be differentiated by the amount of clusters that is growing during the failure process.

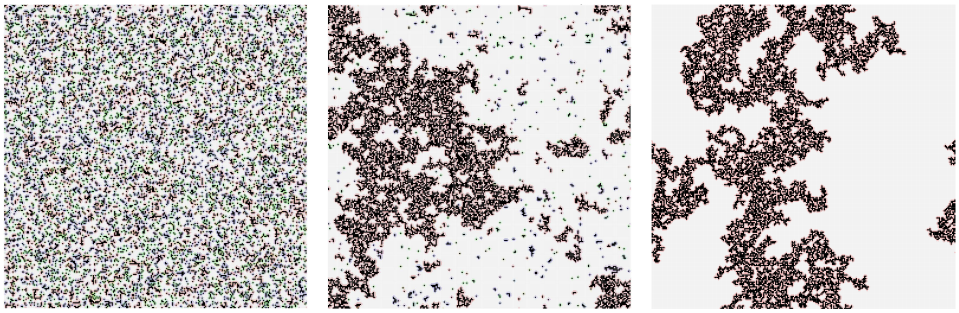

(a) $x_0 = 0$ **(b)** $x_0 = 0.617$ **(c)** $x_0 = 1$

Figure 4.1: *Damage spreading* in the LLS model for various cutoffs in the probability distribution for the failure thresholds of the fibers. The systems have size $N = 256^2$, and the figures shows the broken fibers in the fiber bundle at time step $k/N = 0.2$. The perimeter of each cluster has different colors.

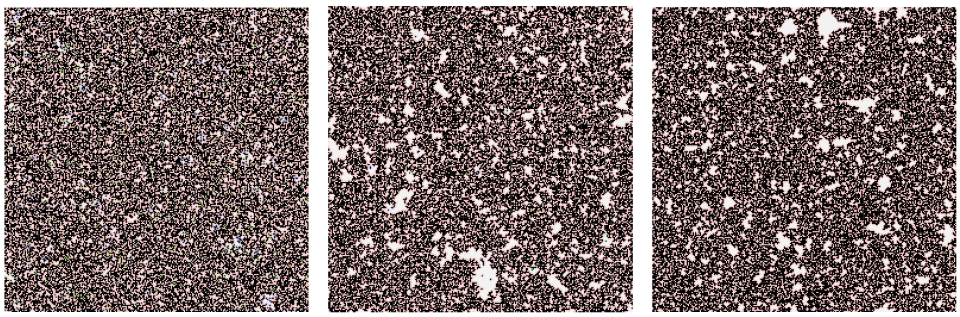

(a) $x_0 = 0$ **(b)** $x_0 = 0.617$ **(c)** $x_0 = 1$

Figure 4.2: *Damage spreading* in the LLS model for various cutoffs in the probability distribution for the failure thresholds of the fibers. The systems have size $N = 256^2$, and the figures shows the broken fibers in the fiber bundle at time step $k/N = 0.58$. The perimeter of each cluster has different colors.

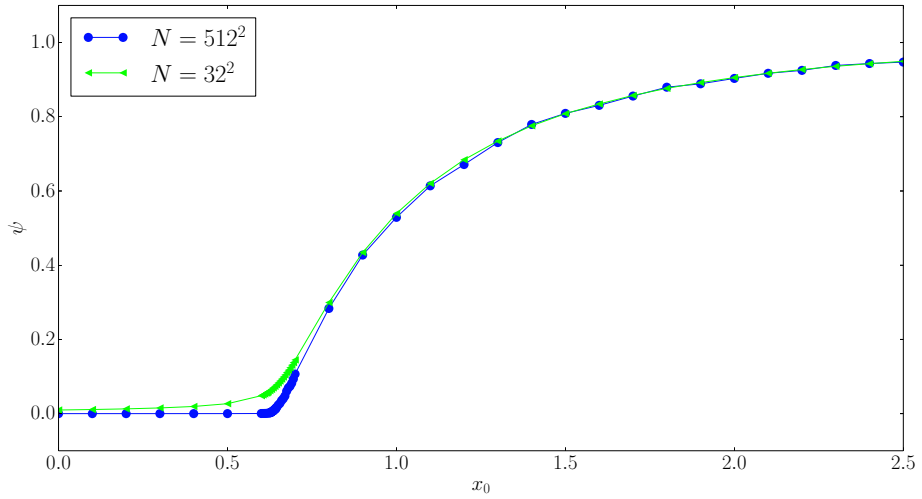

Figure 4.3: *The order parameter:* for systems of size $N = 32^2$ and $N = 512^2$ with cutoffs $x_0 \in [0, 2.5]$. The data is averaged over $2^{30}/N$ samples. Close to the transition, where the frequency of points is higher, the number of samples is doubled.

4.2 The order parameter

In Figure 4.3 the order parameter ψ is shown for a range of cutoffs. The localization transition is easily recognizable. This is a reproduction of results from Dahle (2016). The systems in Figure 4.3 have sizes $N = 32^2$ and $N = 512^2$ and the data is averaged over $2^{30}/N$ samples, except close to the transition where the sample frequency is higher and the number of samples is doubled.

The order parameter was calculated for systems in the range between $N = 4^2$ and $N = 8192^2$, and in Figure 4.4-4.7 the order parameter for cutoffs $x_0 \in [0.616 - 0.618]$ are shown as a function of the system lengths. The dashed line shows a function proportional with $L^{-1.5}$. The data is averaged over $2^{31}/N$ samples.

4.2.1 The next weakest fiber

In the LLS model, the fiber with the lowest failure threshold is always the first to break. In Figure 4.8 the time step k/N at which *the next weakest fiber* breaks is shown for systems of size $N = 32^2$ and $N = 512^2$. The data is averaged over $2^{30}/N$ samples.

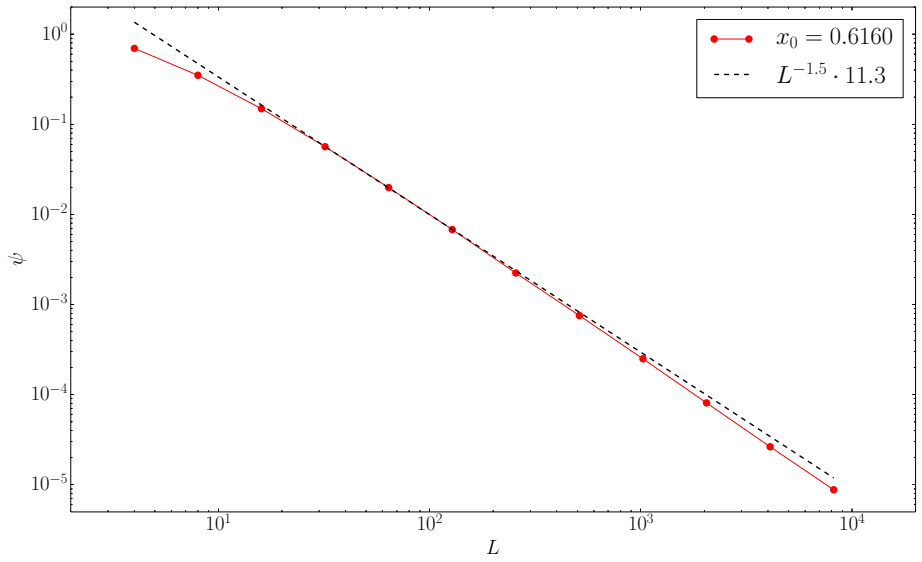

Figure 4.4: *The order parameter* is shown for $x_0 = 0.6160$ for systems of size $N = 4^2$ to $N = 8192^2$. The data is averaged over $2^{31}/N$ samples.

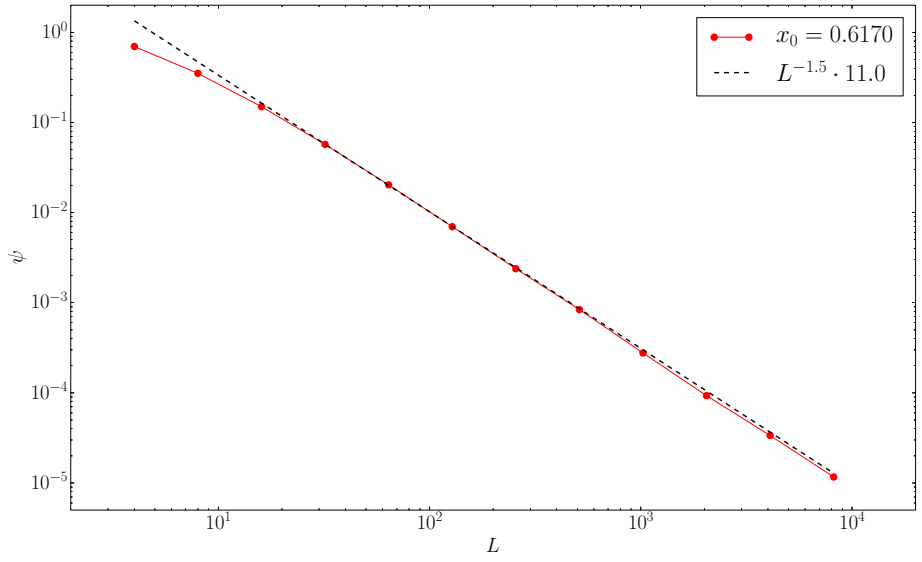

Figure 4.5: *The order parameter* is shown for $x_0 = 0.6170$ for systems of size $N = 4^2$ to $N = 8192^2$. The data is averaged over $2^{31}/N$ samples.

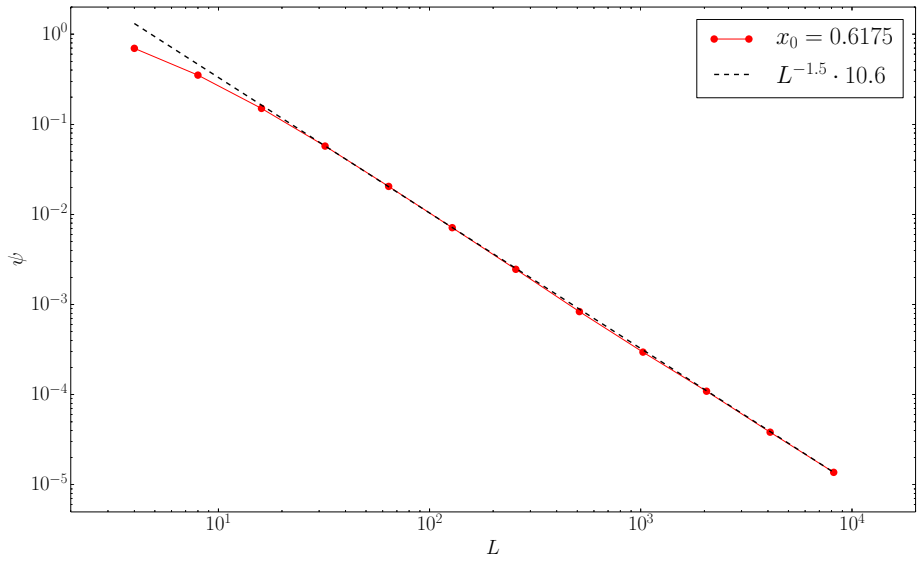

Figure 4.6: *The order parameter* is shown for $x_0 = 0.6175$ for systems of size $N = 4^2$ to $N = 8192^2$. The data is averaged over $2^{31}/N$ samples.

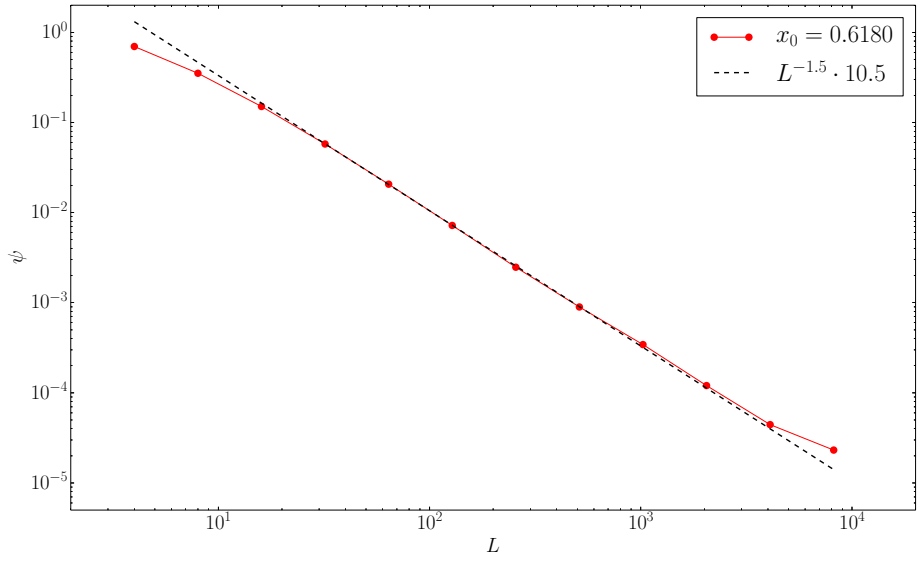

Figure 4.7: *The order parameter* is shown for $x_0 = 0.6180$ for systems of size $N = 4^2$ to $N = 8192^2$. The data is averaged over $2^{31}/N$ samples.

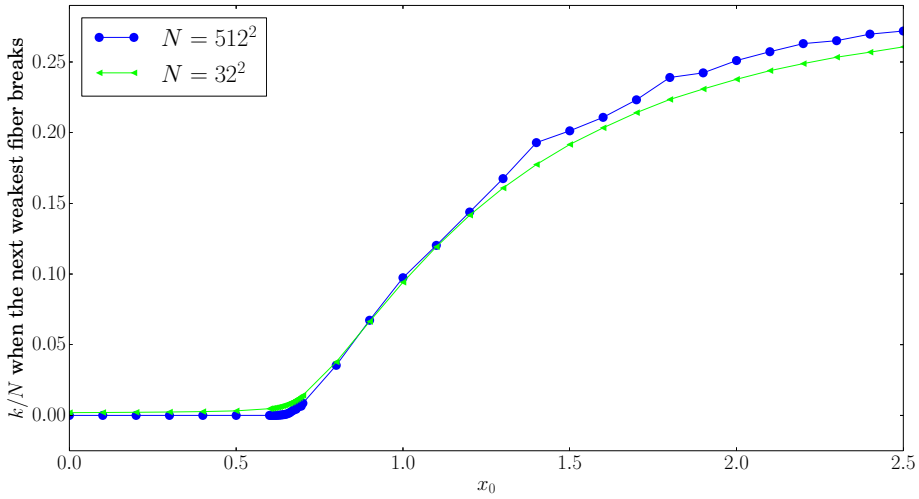

Figure 4.8: *The next weakest fiber:* The time step k/N at which the next weakest fiber in the bundle breaks for systems of size $N = 32^2$ and $N = 512^2$. The data is averaged over $2^{30}/N$ samples.

4.3 The strain curve

In Figure 4.9 the strain curve for the LLS model is shown for cutoffs between 0 and 1 for systems of size $N = 512^2$. The data is averaged over 2^{12} samples. Note that the curve for $x_0 = 0.6$ stands out the most. As opposed to the strain curves for the ELS model with the same threshold distribution seen in Figure 2.3, the LLS model gives rise to a positive slope in the strain curve for $0.4 \lesssim k/N \lesssim 0.6$. This feature appear to be most distinct for $x_0 = 0.6$. In Figure 4.10 a region of the strain curve for $x_0 = 0.617$ is shown for systems of size $N = 64^2$ to $N = 2048^2$. The data is averaged over $2^{30}/N$ samples. The slope is more pronounced for larger system sizes. For comparison with the ELS model, Figure 4.11 displays the strain curve for the LLS system with $x_0 = 0.617$ and size $N = 512^2$ with the analytical strain curve for the ELS model. The standard deviation of the strain curve in the LLS model is shown with a dual axis in red. To illustrate the high fluctuations further, Figure 4.12 display the strain in a single sample compared to the average of 2^{12} samples with $x_0 = 0.5$.

This behaviour is examined more closely in Figure 4.13, where the slope at the inflection point, $\max(\mathrm{d}\sigma/\mathrm{d}k)$, is estimated for cutoffs $x_0 \in [0, 1]$ for systems of size $N = 128^2$ to $N = 512^2$. Each point originates from strain curves with $2^{30}/N$ samples, and close to the maxima, where the frequency of points is higher, the number of samples is doubled. The estimated values originates from fourth

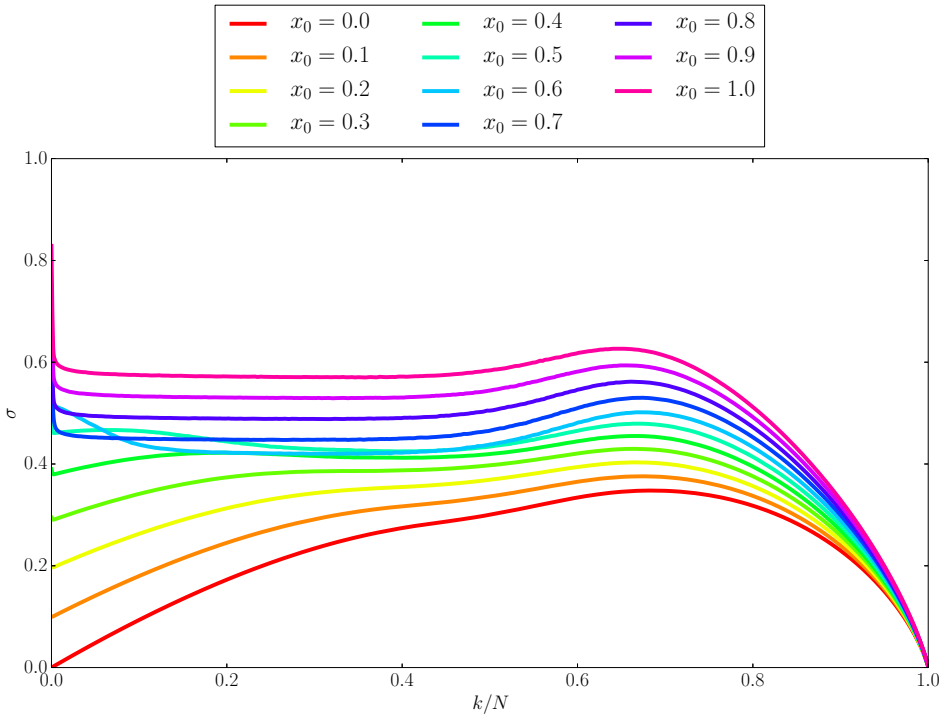

Figure 4.9: *Strain curve for the LLS model* for cutoffs $x_0 \in [0, 1]$. The system have size $N = 512^2$ and the data is averaged over 2^{12} samples.

order polynomial fitting of the strain curves with `numpy.polyfit(...)`[1] in the range $0.4 \leq k/N \leq 0.7$.

Cutoffs $x_0 \in [0.6, 0.7]$ was studied in more detail, this can be seen in Figure 4.14. By preforming second order polynomial fitting of the data close to the maximum values, the respective finite size critical cutoffs x_f was estimated. These curve fitting functions are shown as dashed lines. Interpolation to infinite lattice size is shown in Figure 4.15, which resulted in a critical cutoff $x_c = 0.616 \pm 0.01$.

In Figure 4.16 the stress is shown as a function of the extension of the fiber that breaks for cutoffs $x_0 \in [0, 1]$. In Figure 4.17 this is shown for cutoffs $x_0 \in [1.1, 2.5]$. In Figure 4.18 the force elongation curves for cutoffs $x_0 \in \{0, 0.617, 1\}$ is shown with colors according to the time step at which each fiber breaks.

[1]Documentation: `http://docs.scipy.org/doc/numpy-1.10.0/reference/generated/numpy.polyfit.html`

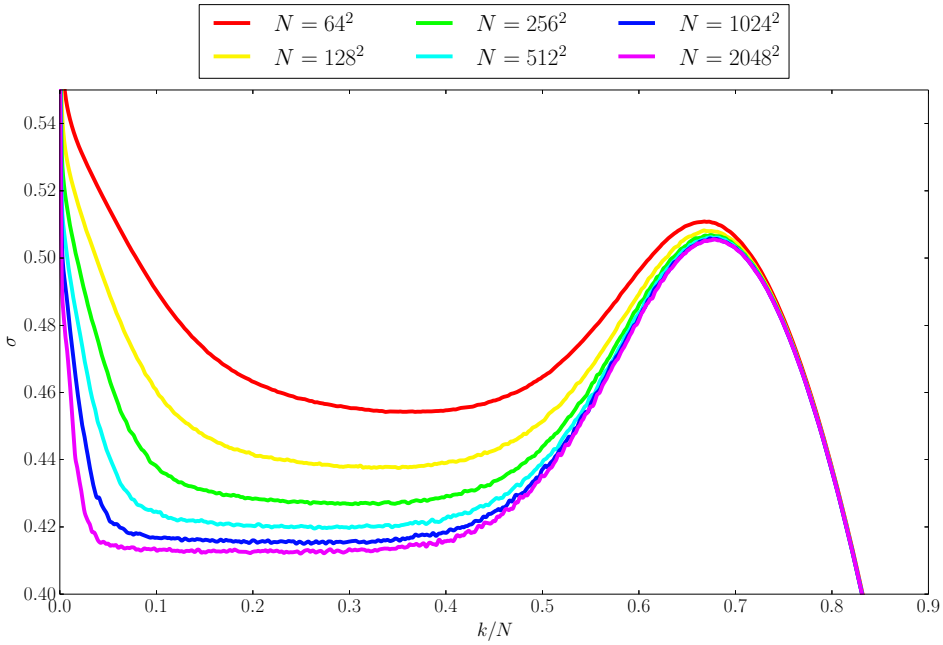

Figure 4.10: *Strain curve for the LLS model* for cutoff $x_0 = 0.617$ for systems of size $N = 64^2$ to $N = 2048^2$. The curves are averaged over $2^{30}/N$ samples.

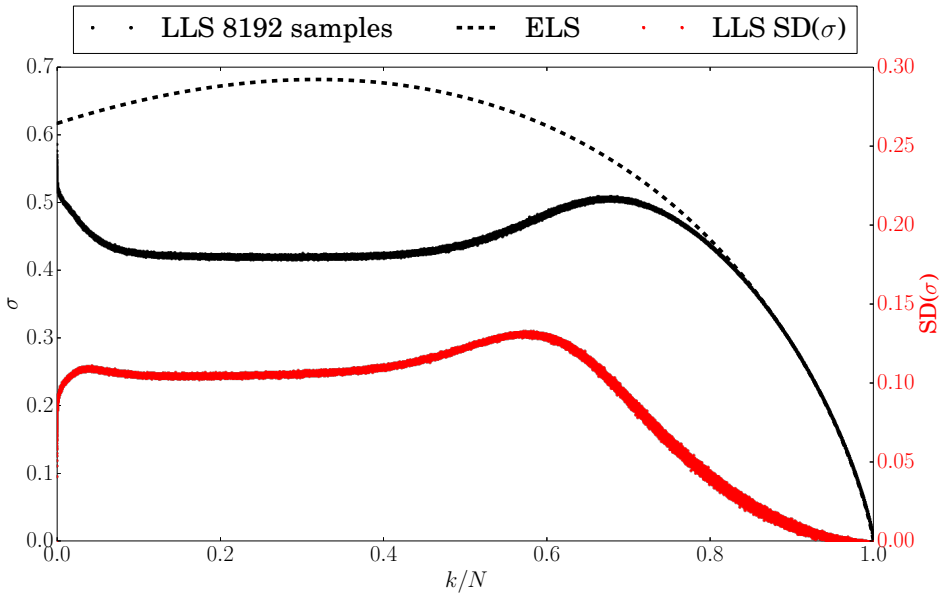

Figure 4.11: *Strain curve for the ELS and LLS model* for cutoff $x_0 = 0.617$. The LLS system has size $N = 512^2$ and is averaged over 2^{13} samples, with corresponding standard deviation shown in red. The analytical strain curve for the ELS model is shown as a dashed line.

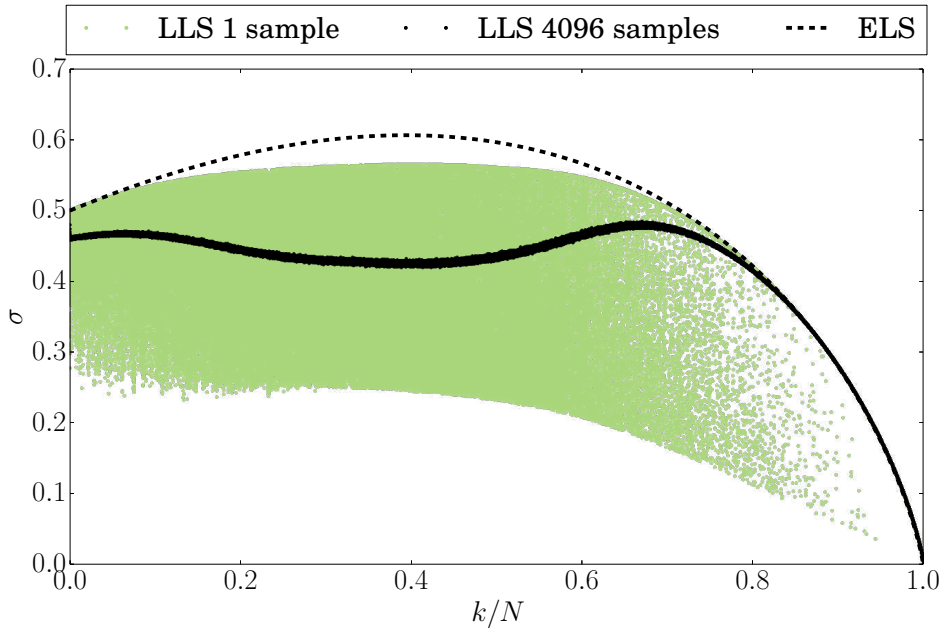

Figure 4.12: *Strain curve for the ELS and LLS model* for cutoff $x_0 = 0.5$. The LLS system has size $N = 512^2$. The green dots display the strain in a single sample, and the black dots are averaged over 2^{12}. The analytical strain curve for the ELS model is shown as a dashed line.

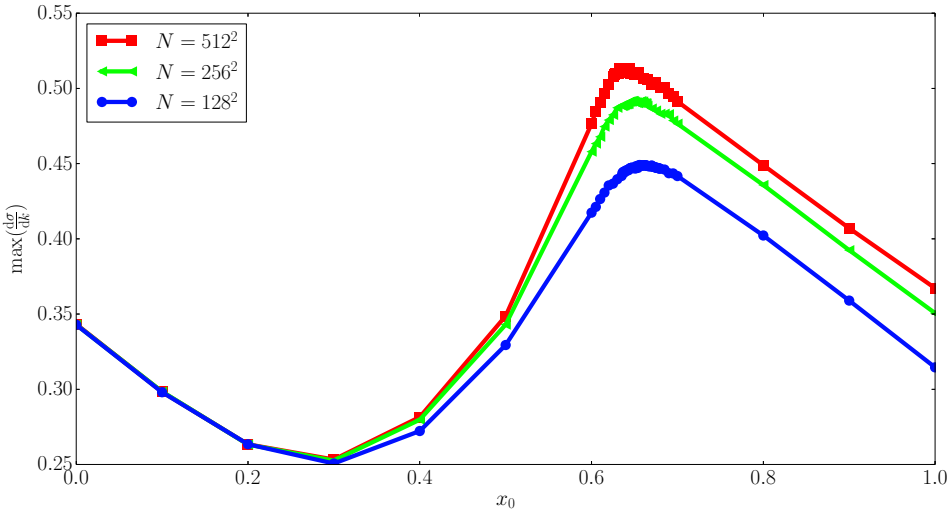

Figure 4.13: *The slope of the strain curve* for various cutoffs $x_0 \in [0, 1]$ for system of size $N = 128^2$ to $N = 512^2$. Each point originates from strain curves with $2^{30}/N$ samples, and close to the maxima, where the frequency of points is higher, the number of samples is doubled.

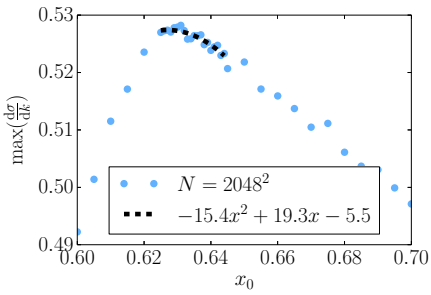

(a) $N = 2048^2$

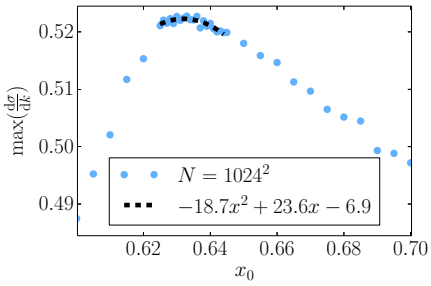

(b) $N = 1024^2$

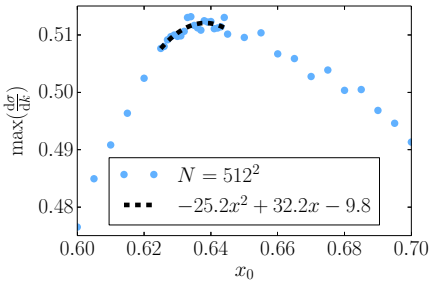

(c) $N = 512^2$

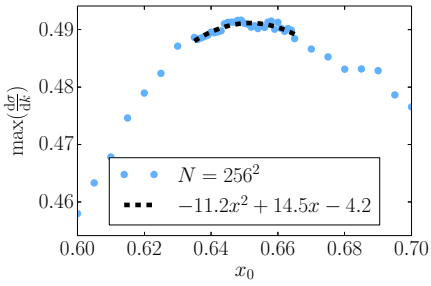

(d) $N = 256^2$

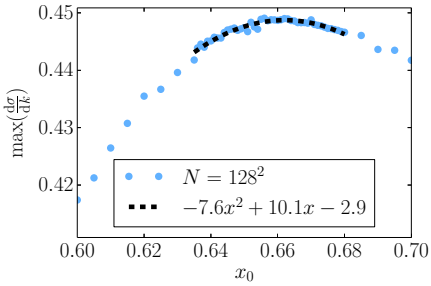

(e) $N = 128^2$

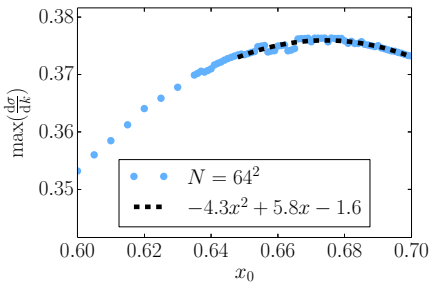

(f) $N = 64^2$

Figure 4.14: *The slope of the strain curve* for various cutoffs x_0 for systems of size $N = 64^2$ to $N = 2048^2$. Each point originates from strain curves with $2^{30}/N$ samples, and close to the maxima, where the frequency of points is higher, the number of samples is doubled. The dashed line shows a second order polynomial fit from which the respective x_f was estimated at the maxima. The length of the interval on the y-axis is equal for all the figures.

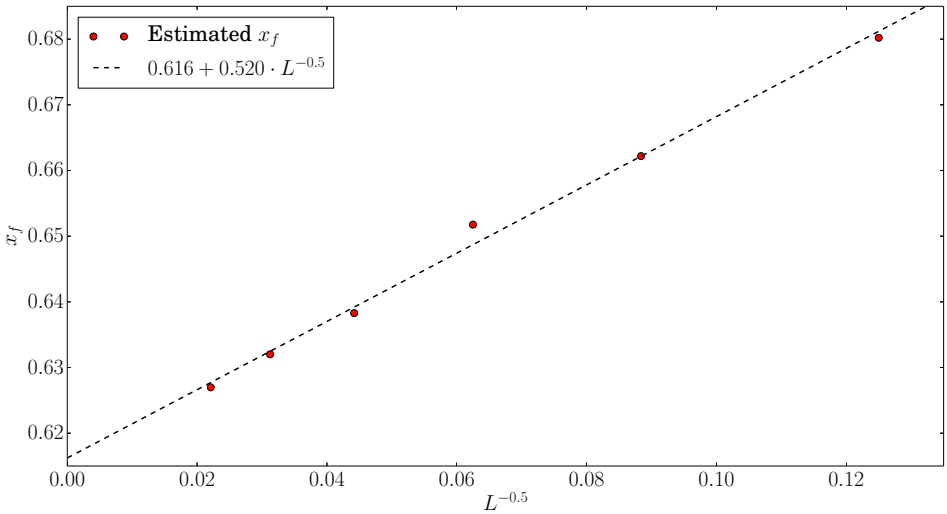

Figure 4.15: *Extrapolation to infinite lattice size:* The critical cutoff x_c was estimated to 0.616 ± 0.01 from the critical finite size cutoffs.

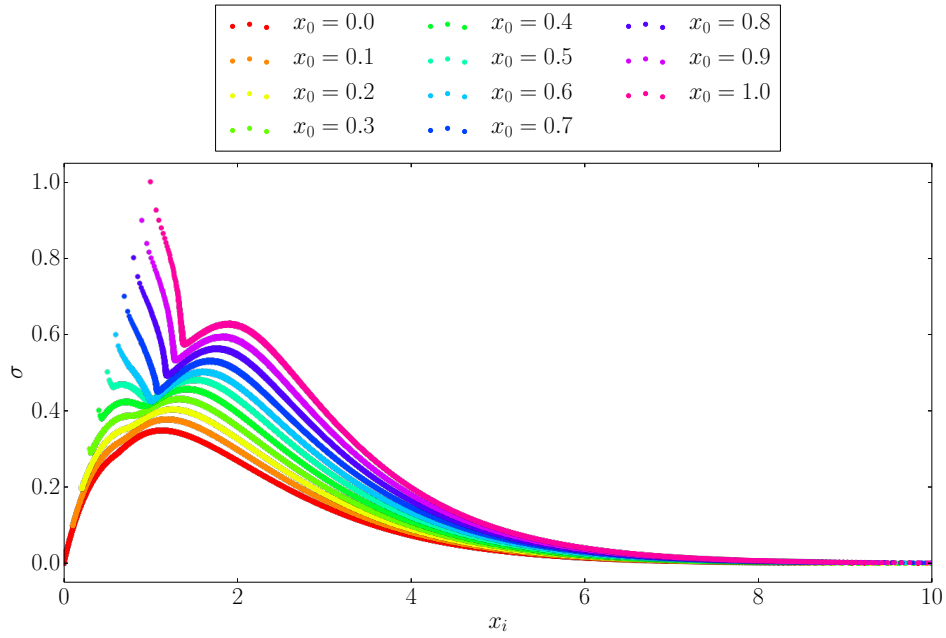

Figure 4.16: *Force against bundle elongation:* The strain on the bundle is shown as a function of the extension of the fiber that breaks for various cutoffs $x_0 \in [0, 1]$. The systems have size $N = 256^2$ and is averaged over 2^{14} samples.

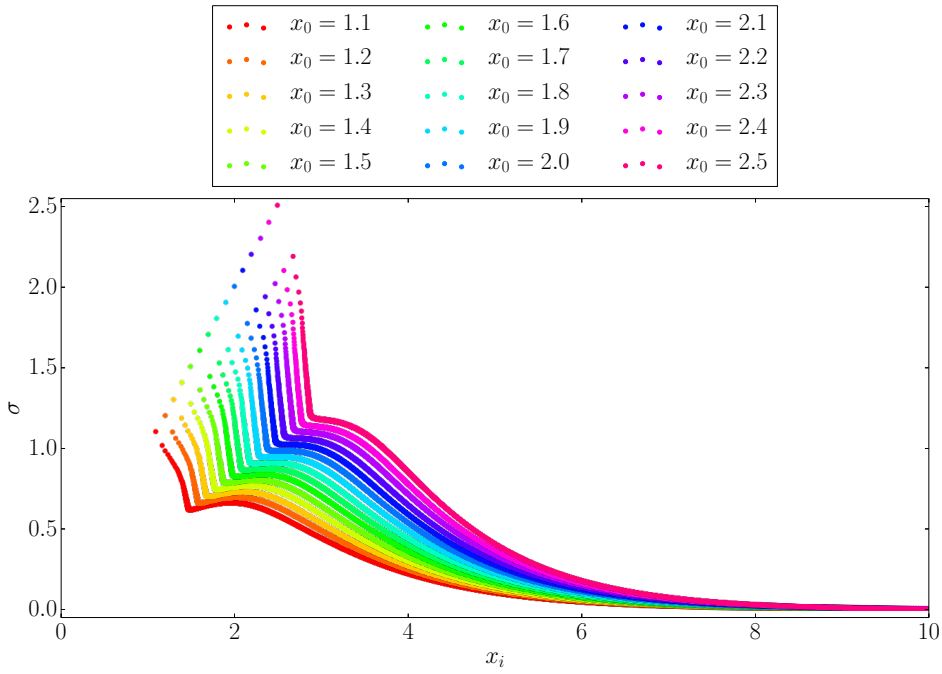

Figure 4.17: *Force against bundle elongation:* The strain on the bundle is shown as a function of the extension of the fiber that breaks for various cutoffs $x_0 \in [1.1, 2.5]$. The systems have size $N = 256^2$ and are averaged over 2^{14} samples.

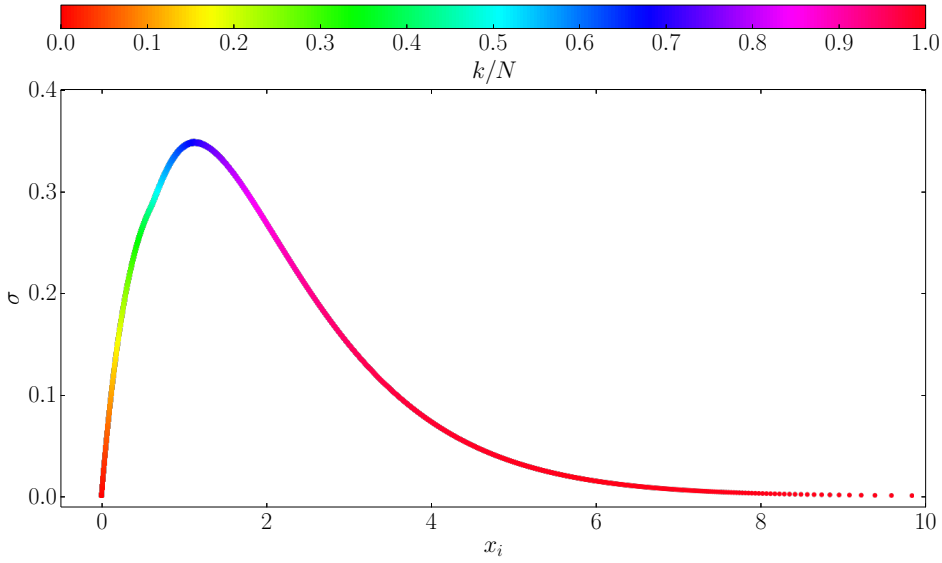

(a) $x_0 = 0$

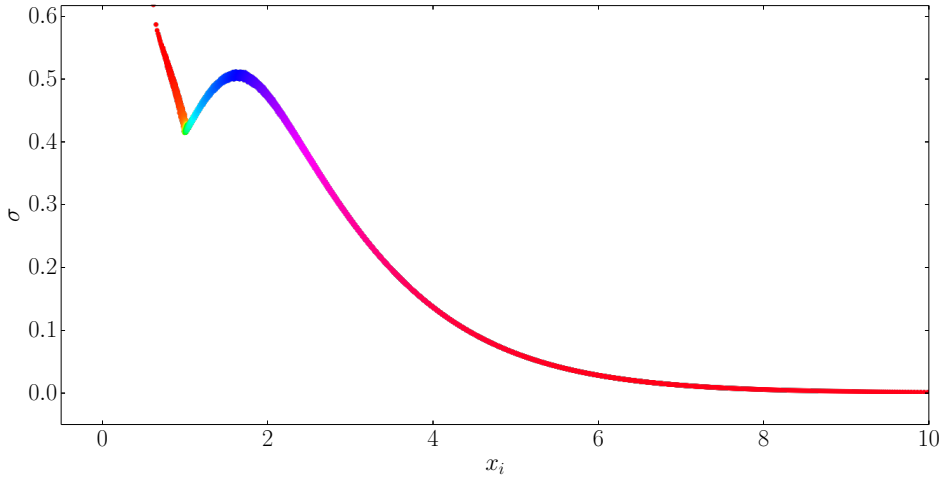

(b) $x_0 = 0.617$

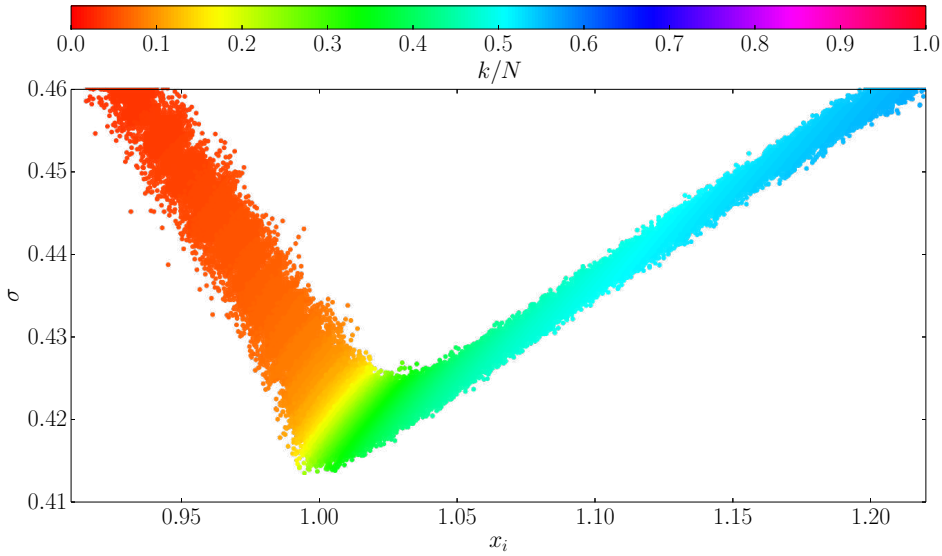

(c) $x_0 = 0.617$, details

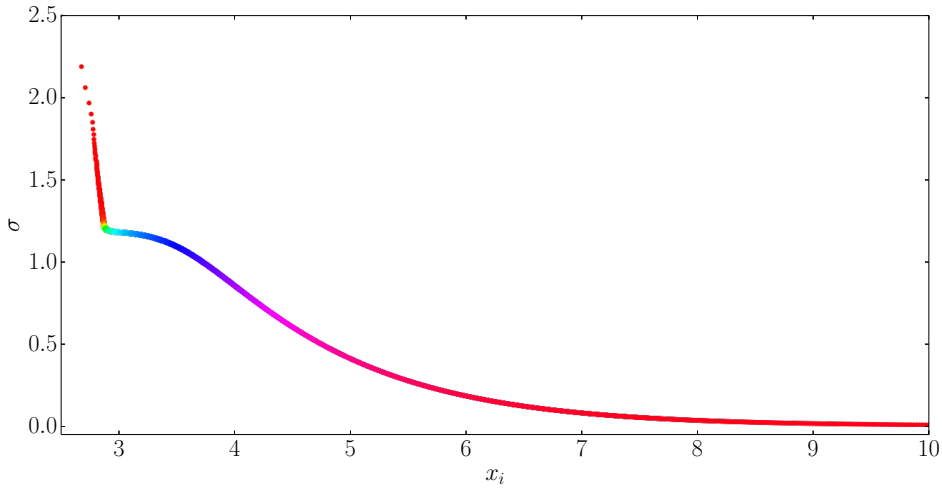

(d) $x_0 = 2.5$

Figure 4.18: *Force against bundle elongation with time:* The strain on the bundle is shown as a function of the extension of the fiber that breaks for cutoffs $x_0 \in \{0, 0.617, 2.5\}$. The systems have size $N = 256^2$ and are averaged over 2^{14} samples. The color bar gives the time step for each data point.

4.4 Burst distribution in the ELS model

The burst distribution in the ELS model was analyzed for various cutoffs. In Figure 4.19 the burst distribution for systems of size $N = 512^2$ is averaged over $2 \cdot 10^6$ samples. By rescaling the y axis with a factor of $\Delta^{5/2}$ and $\Delta^{3/2}$ in Figure 4.19b and Figure 4.19c respectively, the two power law regimes are confirmed. The crossover between these regimes from Equation (2.10) is shown as dashed vertical lines.

The fatal bursts, which break the rest of the bundle, is observed to the lower right in Figure 4.19a. These are shown more clearly in Figure 4.19d. The fatal bursts are expected to be of size $\Delta_{fatal} \approx N - k_{max} = N/e^{1-x_0}$, shown as dotted lines in Figure 4.19d. The non-fatal bursts are included in the normalization. In Figure 4.20 the cumulative probability of a fatal burst occuring is shown. This emphasizes the criticality occurring when $x_0 = 1$, for which the strain curve is monotonically decreasing. With this cutoff about 1.5% of the fatal bursts are initiated by the first fiber that breaks.

To illustrate the burst distribution above criticality, Figure 4.21 shows the burst distribution for the ELS model with $x_0 \in [1.1, 2]$.

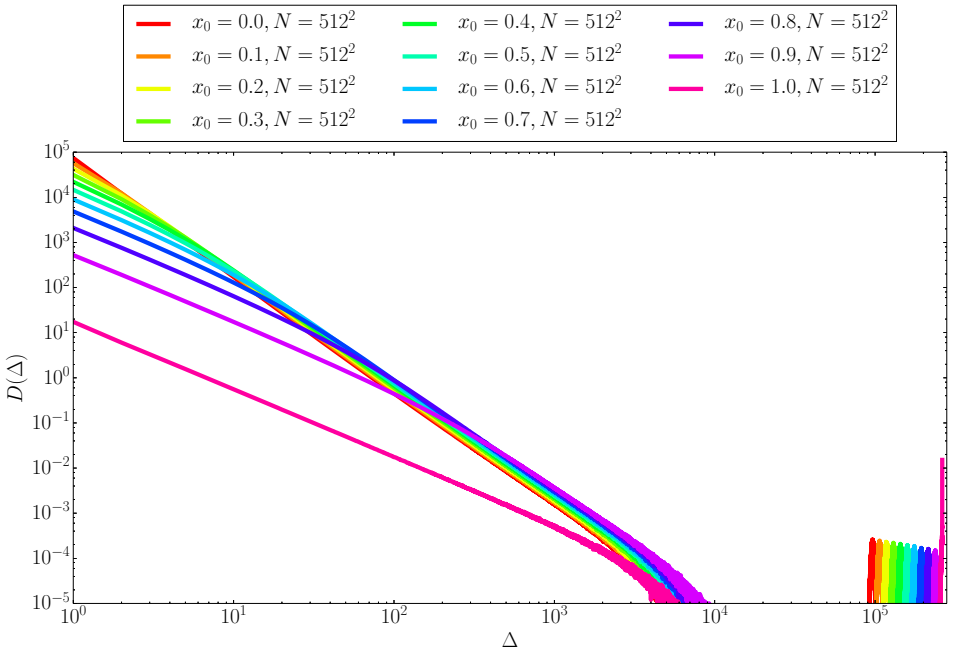

(a) *The burst distribution for the ELS model* for cutoffs $x_0 \in [0, 1]$.

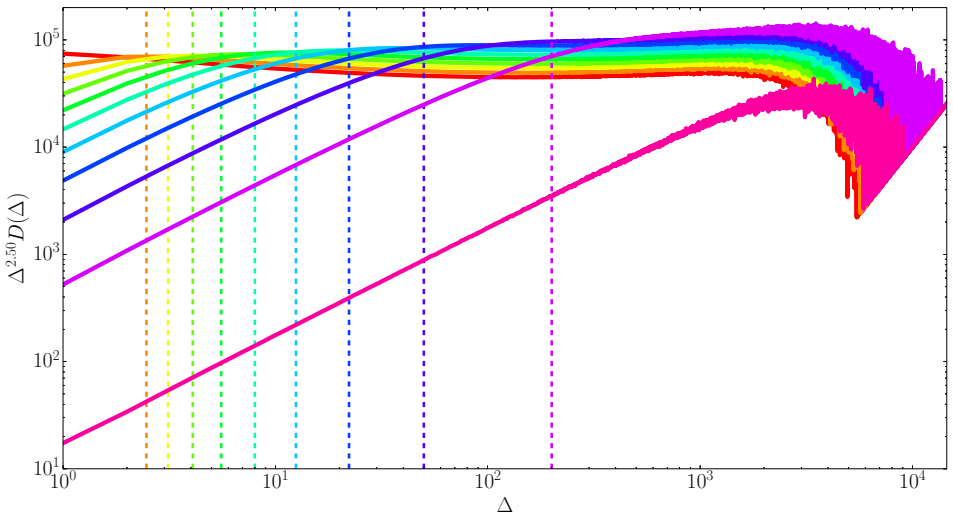

(b) *The ELS burst distribution scaled with a factor* $\Delta^{2.50}$. Vertical lines shows Δ_c.

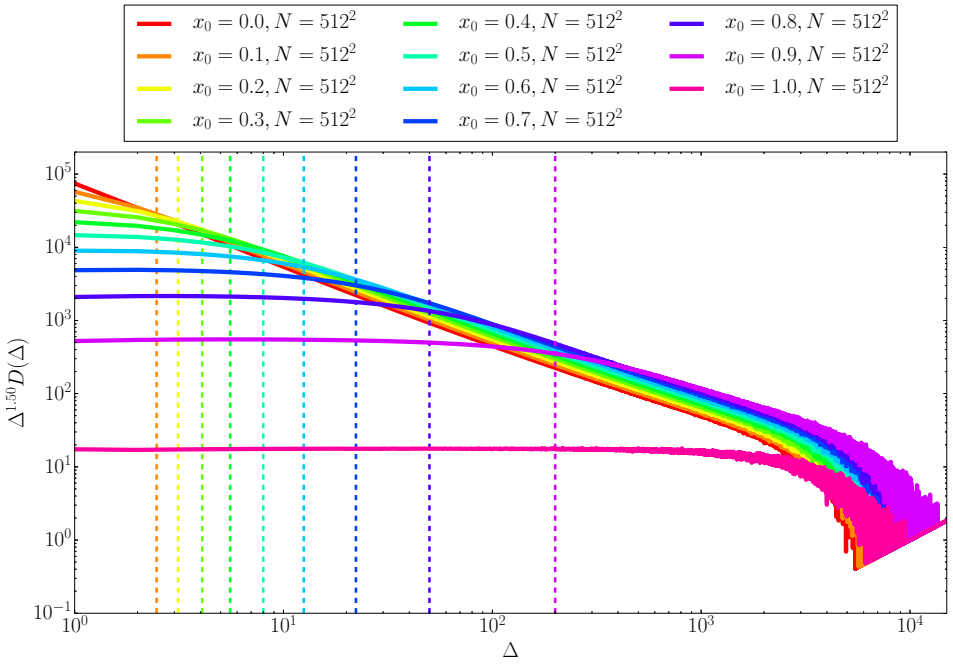

(c) *The ELS burst distribution scaled with a factor* $\Delta^{1.50}$. Vertical lines shows Δ_c.

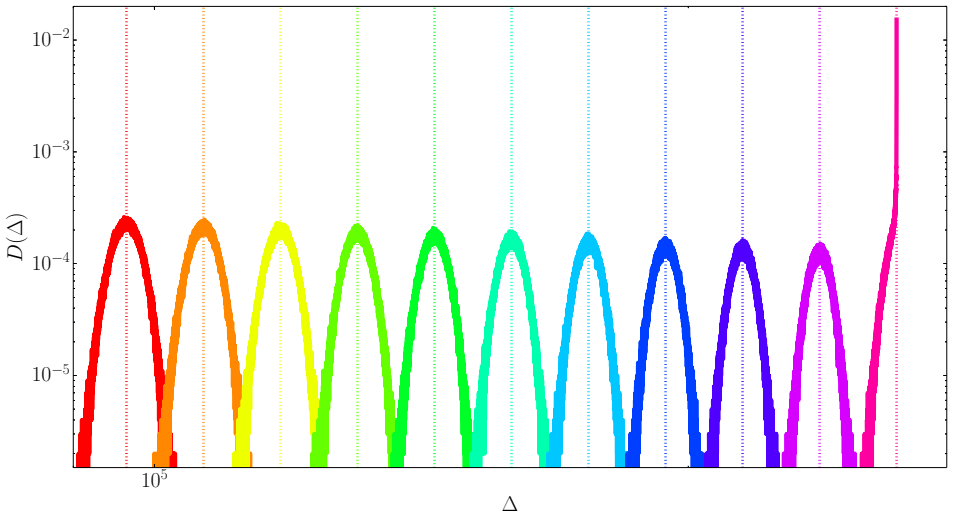

(d) *Fatal bursts* in the ELS model. Dotted vertical lines shows burst of size $\Delta = N/e^{1-x_0}$.

Figure 4.19: *Burst distribution for the ELS model* for cutoffs $x_0 \in [0, 1]$. The results are averaged over $2 \cdot 10^6$ samples of systems with size $N = 512^2$.

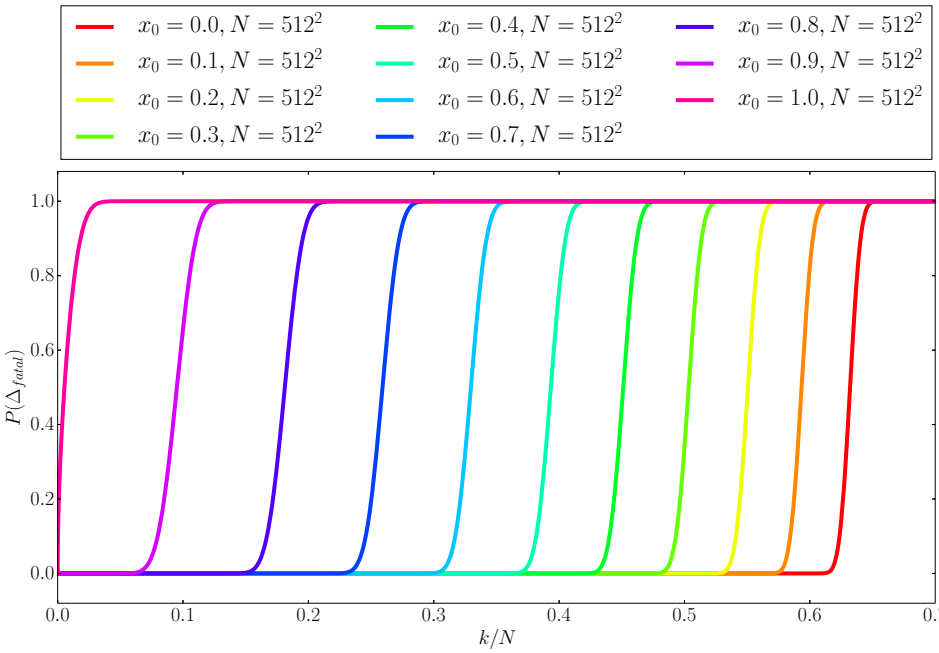

Figure 4.20: *Fatal bursts in the ELS model:* The cumulative probability of a fatal burst in the ELS model is shown for $x_0 \in [0, 1]$ for systems of size $N = 512^2$.

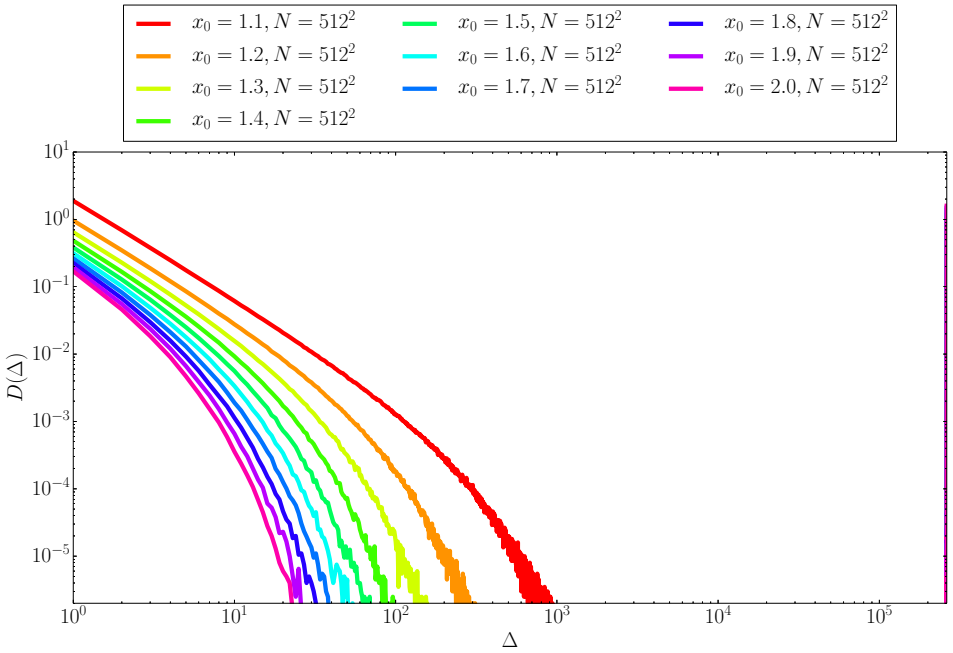

(a) *The burst distribution for the ELS model* for cutoffs $x_0 \in [1.1, 2]$.

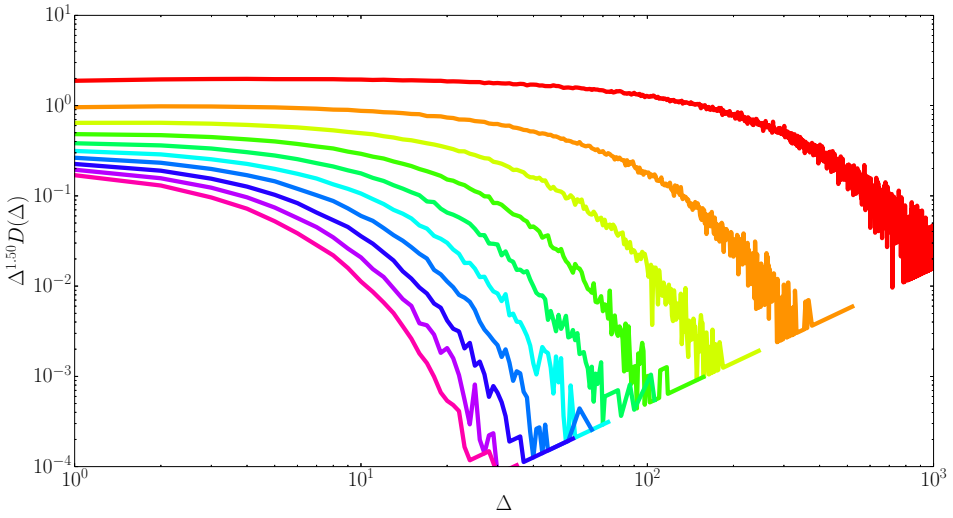

(b) *The ELS burst distribution scaled with a factor* $\Delta^{1.50}$.

Figure 4.21: *Burst distribution for the ELS model* for cutoffs $x_0 \in [1.1, 2]$. The results are averaged over $2 \cdot 10^6$ samples of systems with size $N = 512^2$.

4.5 Burst distribution in the LLS model

In Figure 4.22-4.25 the burst distribution for the LLS model is shown for cutoffs between 0 and 1 for systems of size $N = 512^2$. The systems with $x_0 \in [0, 0.5]$ are averaged over 2^{12} samples, and the systems with $x_0 \in [0.6, 1]$ are averaged over 2^{16} samples. This difference is due to the fact that the occurrences of nonfatal burst decrease as the cutoff is increased. Moreover, the simulation program is significantly faster for cutoffs above x_c. To avoid data collapse, the curves are divided into several figures. The systems with cutoffs in the interval $x_0 \in [0, 0.2]$ seen in Figure 4.23b does not match well with a power law of $\tau = 2$. As the cutoff is increased, the fit is moderately better. Note that the power law fit is best for cutoffs around the critical transition. From Figure 4.25b it appears as though the burst distribution falls off faster as the cutoff approaches $x_0 = 1$. In Figure 4.26, the burst distribution for $x_0 = 0.617$ is calculated for systems of size $N = 64^2$ to $N = 4096^2$. Large systems provides results that are consistent with $\tau = 2.0$, while smaller systems appear have a slightly smaller exponent. This may be compared to the behaviour for $x_0 = 0$, as shown in Figure 4.27. To investigate the power law behaviour with no cutoff, the burst distribution is scaled to fit a power law $D(\Delta) \sim \Delta^{\tau}$, with $\tau = 2.37$ and $\tau = 2.37$ in Figure 4.27c and 4.27b respectively. The size of the interval on the y-axis is equal to that of Figure 4.26b to simplify the comparison.

4.5.1 Fatal bursts in the LLS model

In Figure 4.28 the cumulative probability of a fatal burst to occur during the failure process, $P_{\Delta_{fatal}}$, is seen for $x_0 \in [0, 1]$ for systems of size $N = 512^2$. The data is averaged over $2^{30}/N$ samples. For $x_0 = 0$ the mean onset of a fatal burst is at about $k/N = 0.65$. For comparison, the strain curve for $N = 512^2$ with $x = 0$ has a global maximum around $k/N = 0.687$. For $x_0 = 1$ more than 30% of the fatal bursts are initiated by the first fiber that breaks. The finite size effects is elaborated in Figure 4.29, which shows $P_{\Delta_{fatal}}$ for systems of size $N = 64^2$ to $N = 2048^2$ with $x_0 = 0.617$. The data is averaged over $2^{31}/N$ samples.

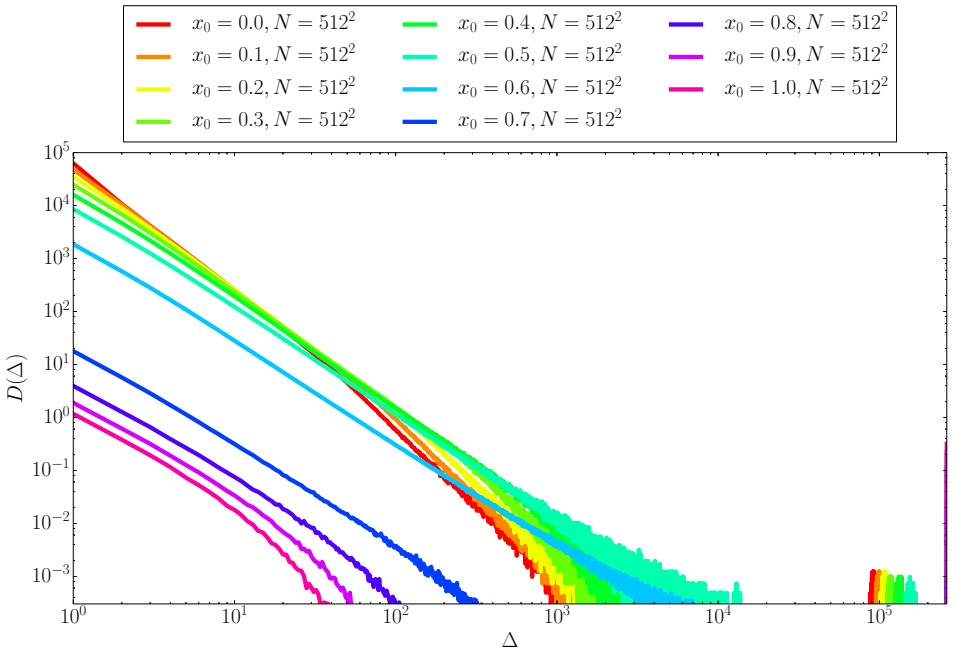

Figure 4.22: *Burst distribution for the LLS model* for cutoffs $x_0 \in [0, 1]$ for systems of size $N = 512^2$. The systems with $x_0 \in [0, 0.5]$ are averaged over 2^{12} samples, and the systems with $x_0 \in [0.6, 1]$ are averaged over 2^{16} samples.

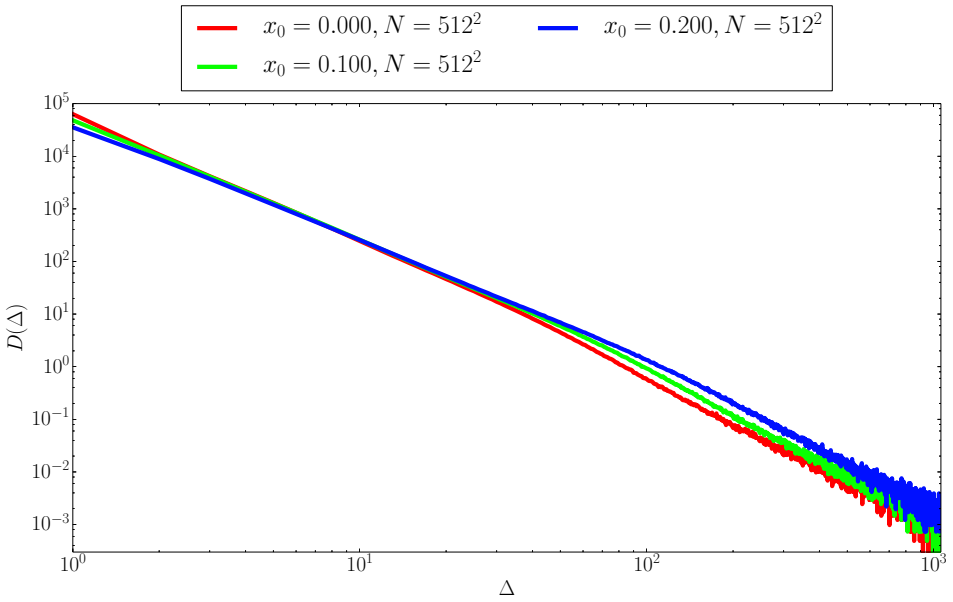

(a) *The burst distribution for the LLS model* for cutoffs $x_0 \in [0, 0.2]$.

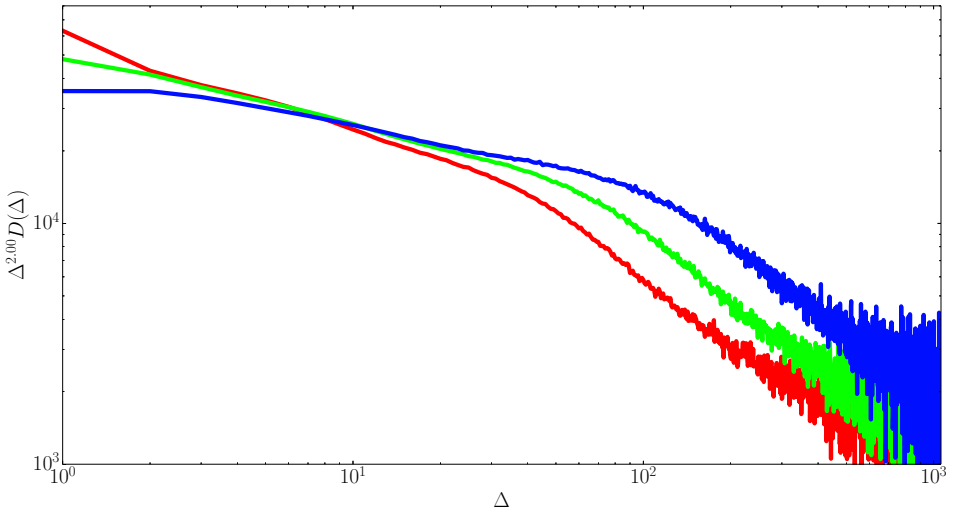

(b) The LLS burst distribution scaled with a factor $\Delta^{2.00}$.

Figure 4.23: *Burst distribution for the LLS model* for cutoffs $x_0 \in [0, 0.2]$ for systems of size $N = 512^2$. The data is averaged over 2^{12} samples.

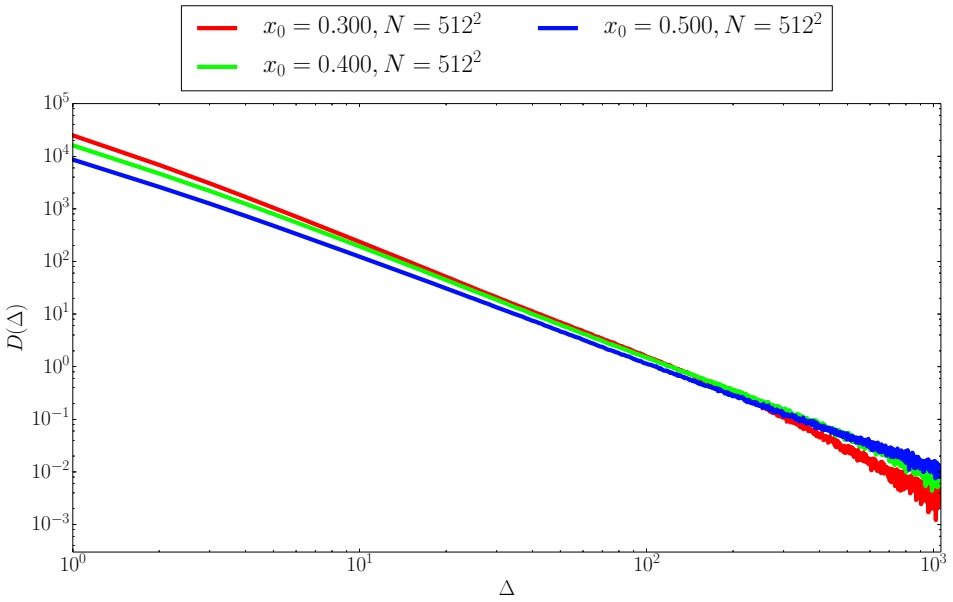

(a) *The burst distribution for the LLS model* for cutoffs $x_0 \in [0.3, 0.5]$.

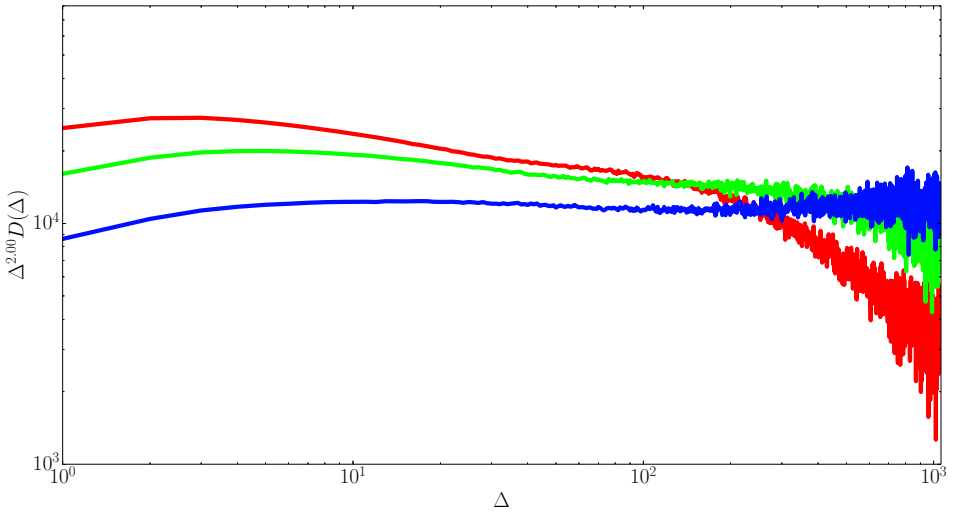

(b) *The LLS burst distribution scaled with a factor* $\Delta^{2.00}$.

Figure 4.24: *Burst distribution for the LLS model* for cutoffs $x_0 \in [0.3, 0.5]$ for systems of size $N = 512^2$. The data is averaged over 2^{12} samples.

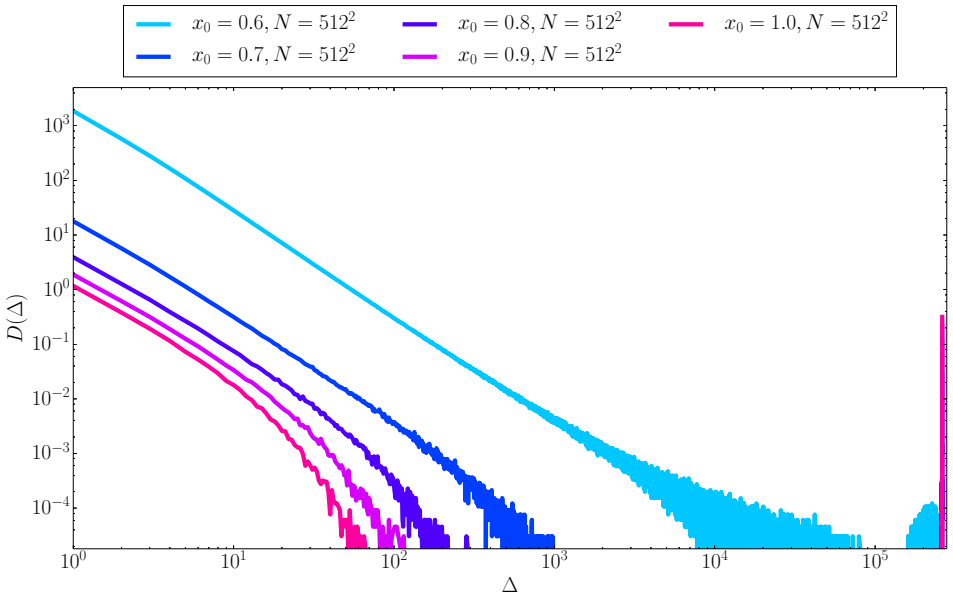

(a) *The burst distribution for the LLS model* for cutoffs $x_0 \in [0.6, 1]$.

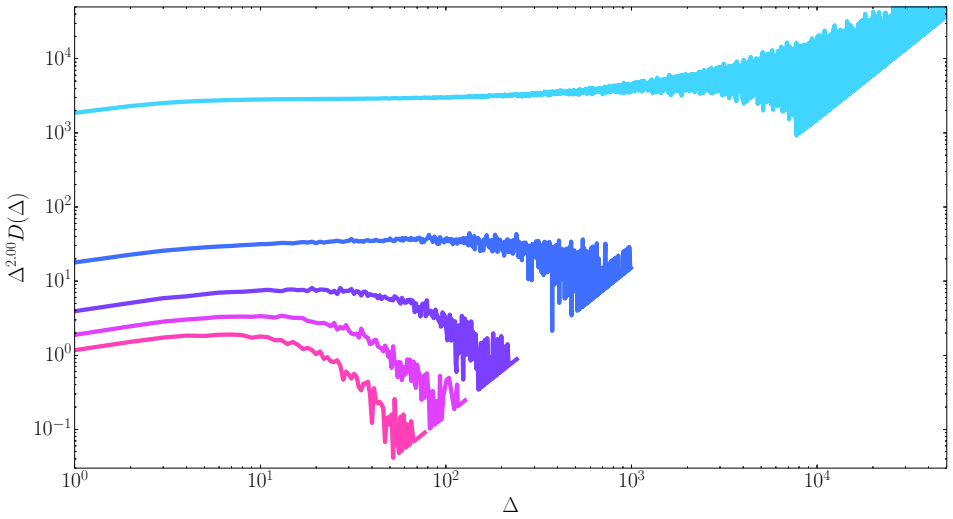

(b) *The LLS burst distribution scaled with a factor* $\Delta^{2.00}$.

Figure 4.25: *Burst distribution for the LLS model* for cutoffs $x_0 \in [0.6, 1]$ for systems of size $N = 512^2$. The data is averaged over 2^{16} samples.

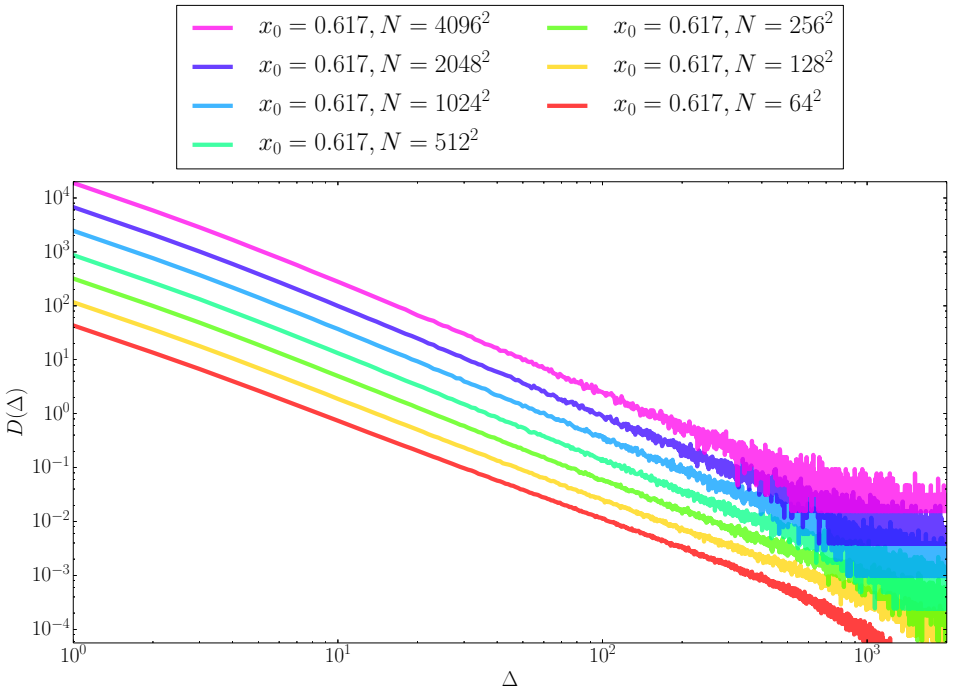

(a) *The burst distribution for the LLS model* for cutoff $x_0 = 0.617$.

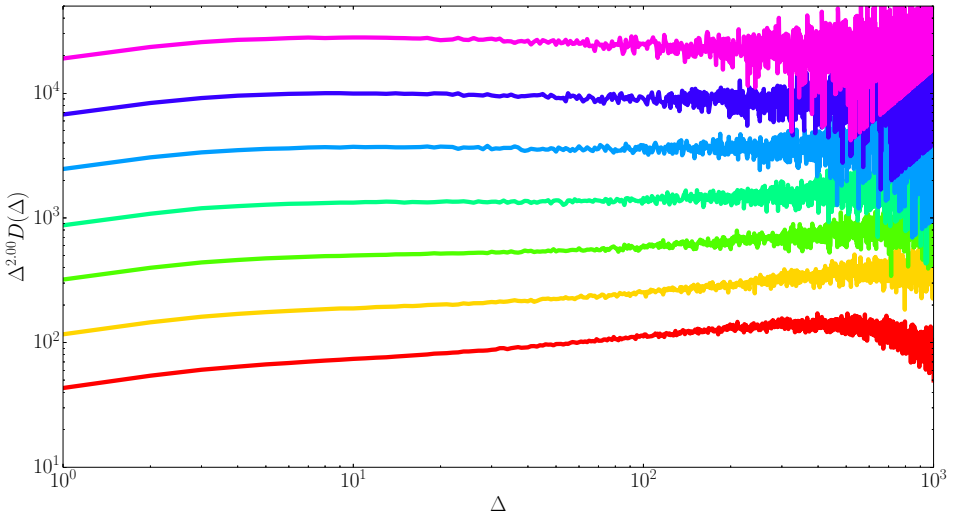

(b) *The LLS burst distribution scaled with a factor* $\Delta^{2.00}$.

Figure 4.26: *The burst distribution for the LLS model* for $x_0 = 0.617$ for systems of size $N = 64^2$ to $N = 4096^2$. The data is averaged over $2^{30}/N$ samples.

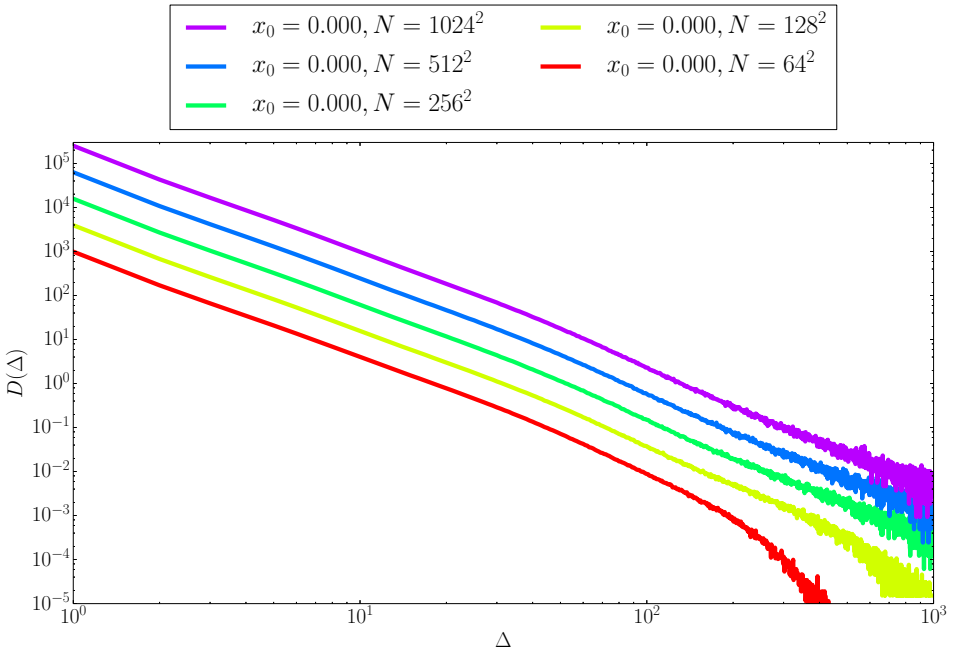

(a) *The burst distribution for the LLS model* for cutoff $x_0 = 0$.

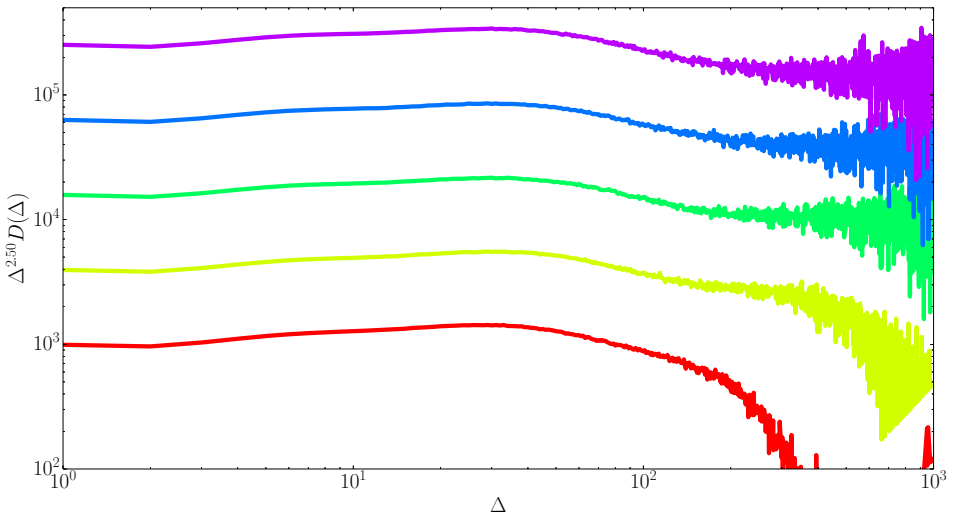

(b) *The LLS burst distribution scaled with a factor* $\Delta^{2.5}$.

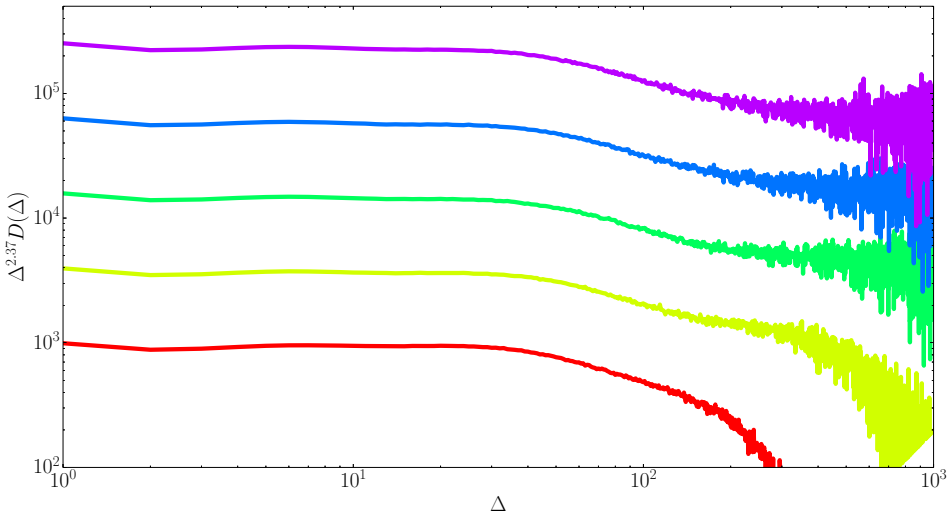

(c) *The LLS burst distribution scaled with a factor* $\Delta^{2.37}$.

Figure 4.27: *The burst distribution for the LLS model* for $x_0 = 0$ for systems of size $N = 64^2$ to $N = 1024^2$. The data is averaged over $2^{30}/N$ samples.

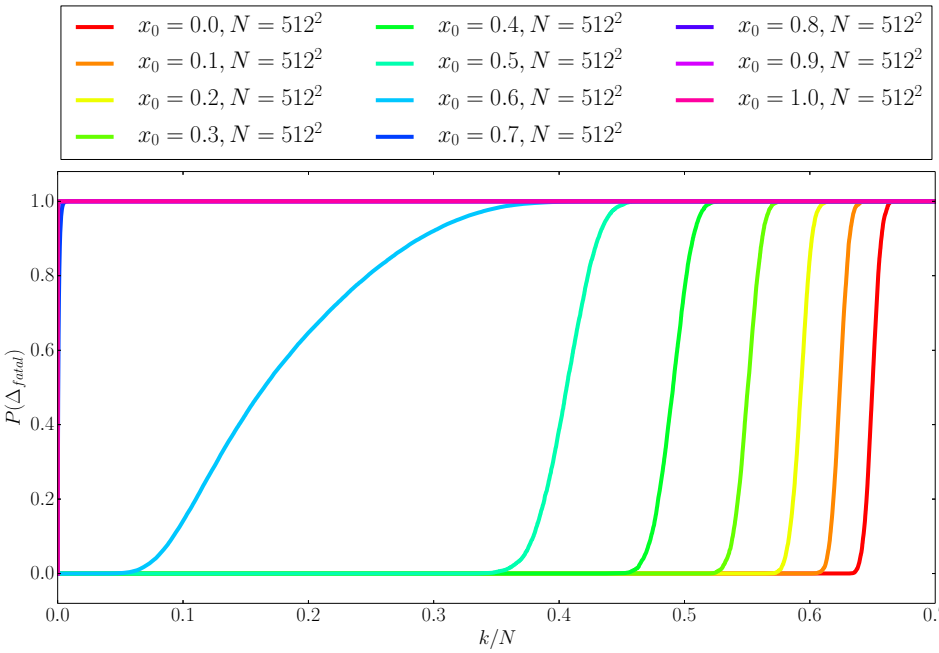

Figure 4.28: *Fatal bursts in the LLS model:* The cumulative probability of a fatal burst in the LLS model is shown for $x_0 \in [0, 1]$ for systems of size $N = 512^2$. The systems with $x_0 \in [0, 0.5]$ are averaged over 2^{12} samples, and the systems with $x_0 \in [0.6, 1]$ are averaged over 2^{16} samples.

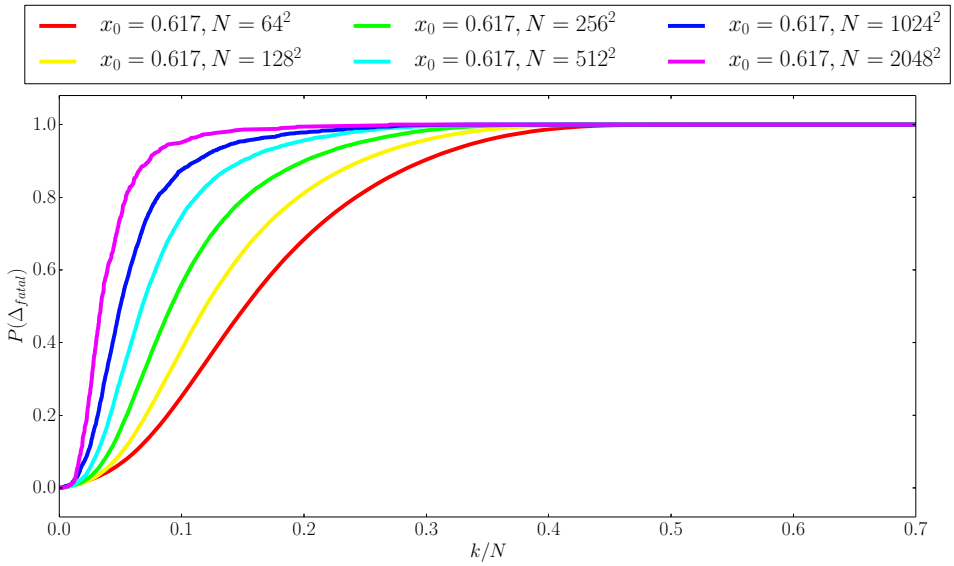

Figure 4.29: *Fatal bursts in the LLS model:* The cumulative probability of a fatal burst in the LLS model is shown for $x_0 = 0.617$ systems of size $N = 64^2$ to $N = 2048^2$. The data is averaged over $2^{31}/N$ samples.

Chapter 5

Discussion

This section discuss and interpret the implications and validity of the results presented in Chapter 4. By analyzing the impact of the cutoff x_0 in the exponential distribution $P(x) = 1 - e^{-x+x_0}$ for the failure thresholds of the fibers, a critical phase transition is identified and investigated. This is linked to a local stability in the LLS model which is not present in the ELS model. A system is here said to be locally stable in the region where the averaged strain curve has a positive derivative. The burst distribution is discussed for both models, and the LLS model is shown to undergo a drastic loss of global stability around the localization transition, in the sense that far fewer fibers may break before catastrophic failure is to be expected in a force controlled experiment.

5.1 The existence of a phase transition

Figure 4.1 gives a qualitative summary of how the fiber bundle systems change behaviour for different cutoffs. The system with $x_0 = 0$ represents the disordered phase, and resembles the ELS model. The cutoff sets a lower limit for the failure threshold of the fibers. When the cutoff is increased, the ratio between the weak and the strong fibers decrease. Localization occurs when the effective thresholds for the fibers neighbouring a cluster is lower than the failure threshold of the weak fibers in the bundle. With sufficiently high cutoff, all the broken fibers belong to the same cluster. This represents the ordered phase, and is illustrated with $x_0 = 1$ in Figure 4.1c. Between these regimes, the LLS model appear to undergo a critical transition, studied more in depth in Section 5.2. The bundle state at time step $k/N = 0.2$ for $x_0 = 0.617$, as shown in Figure 4.1b, indicates that the system is in the vicinity of a critical transition.

5.2 The order parameter

From Figure 4.1 it is obvious that the number of clusters in the simulation is a quantity that is strongly related to the degree of localization. By introducing the order parameter ψ from Equation (2.17), defined as the inverse maximum of the amount of clusters in the simulation, the phase transition may be investigated in more detail. In Figure 4.3 the order parameter is shown for cutoffs in the range between 0 and 2.5 for systems of size $N = 32^2$ and $N = 512^2$. From the sharp transition around $x_0 \approx 0.6$ it is evident that the LLS model has a critical transition around this value.

Dahle (2016) estimated the critical cutoff by locating the steepest slope in the curves for the order parameter plottet against x_0 for each system size. Alternatively, one may exploit the relation from Equation (2.16), i.e. the fact that the order parameter scales as the inverse system length to the power of the critical exponent β/ν very close to the critical point. From this both the critical point and the critical exponent was found.

The order parameter was calculated for systems of size $N = 4^2$ to $N = 8192^2$ for various cutoffs, this is shown in Figure 4.4-4.7. The order parameter for $x_0 = 0.616$ appears to fall off faster than a power law for large system sizes. The opposite is seen in Figure 4.7, where $x_0 = 0.618$ seems to give rise to an upward curvature in the logarithmic plot. The order parameter $x_0 = 0.617$ and $x_0 = 0.6175$ appear to have the best fit to a power law with respect to the inverse system length, suggesting that x_c is closer to 0.6173. From this the critical exponent was estimated to $\beta/\nu = 1.5 \pm 0.1$. This is in accordance with Dahle (2016). The result may be compared with the exponents for percolation, where $\beta/\nu = 5/48 \approx 0.11$, cf. Sykes *et al.* (1974) and Lorenz and Ziff (1998). From this it is clear that the LLS model belongs to a different universality class than percolation. With percolation, there is no interaction between occupied and unoccupied lattice sites, however this is not the case for the LLS fiber bundle model. With this in mind, the different universality classes is perhaps less alarming.

A critical transition may be described by multiple order parameters. By averaging the time steps at which the next weakest fiber in the bundle breaks, this might also suffice as an order parameter. Without cutoff, the next weakest fiber is always the second fiber to break. For higher cutoff, the distribution of fiber strength is no longer strong enough to compete with the stress-enhancement due to local load sharing. As seen in Figure 4.8, the behaviour of this quantity is similar to ψ. The fluctuations do however appear to be more significant. Moreover, large systems need about the same amount of samples as smaller systems, and hence ψ was the preferred order parameter.

5.3 Local stability

Consider a system at the localization transition. When the external load on the bundle is increased, the weak fibers throughout the bundle break. This induces separate fractures which grow throughout the bundle. Figure 4.1b displays the system state around the percolation transition, when the largest cluster is spanning the entire system. The fractal nature of the growing cluster is obvious. Similar to how a river erodes its way through the landscape, the largest cluster branches out in the direction that offers the least resistance. This leave collections of intact fibers encapsulated by walls of fibers with higher failure threshold. As more fibers break, the intact fibers have the appearance of islands in an ocean of broken fibers, as seen in Figure 4.2b.

When the growing cluster has no new areas to spread to, it is forced to tear down the walls of strong fibers. This expose the collections of intact fibers with lower failure threshold, that typically collapse at once upon interaction with the growing cluster. This process gives rise to high fluctuations, and causes the average external load on the bundle to increase. This also explains the maximum in the curve for the standard deviation of the strain curve seen in Figure 4.11. As the cluster grows, an increasing proportion of the intact fibers is included in the perimeter. When $k/N \approx 0.8$, almost all the intact fibers are located along the perimeter of the largest cluster, and the behaviour resembles the ELS model. This final stage of the failure process is identical for all cutoff values.

In the ELS model, all the fibers experience an increased load as more fibers break. When the load of the broken fibers are distributed locally among the nearest intact neighbours, only the strong fibers in the perimeter remain intact. The strong fibers thus adopt a greater load than the weak fibers, resulting in a model with higher local stability. This effective shielding of weak fibers is in excellent agreement with the qualitative explanation presented by Kjellstadli in the early stages of this assignment.

With no cutoff, the difference in fiber strength is small compared to the stress-enhancement near the clusters due to local load sharing. However, as the clusters grow, the stress in the perimeters increase, and cause the same effect as outlined above, though the stable region is less pronounced. When the cutoff is sufficiently high, the failure process is localized from the beginning. As there are no weak fibers, the bundle is able to withstand a greater external force before breaking down. The stable region is completely absent, as the load from the broken fibers are completely dominating over the difference in fiber strength.

In Figure 4.16 the strain on the bundle is shown as a function of the extension of the fiber that breaks for a range of cutoffs. As the cutoff is increased, a discontinuity is emerging in this force-elongation curve. However, the abrupt change

seen around $x_i \approx 1$ in Figure 4.16 might be misleading. As revealed by Figure 4.18, about 30% of the failure process is condensed within this small region of the curve. The onset of the local stability appear to succeed the occurrence of a spanning cluster, and originates from the same mechanism as outlined above. The following stability disappear for sufficiently high cutoff, as seen in Figure 4.17.

This stability is also apparent from the strain curve. The slope of the strain curve is studied exhaustively in Figure 4.13-4.15.

By investigating the slope of the strain curve for various system sizes, this provides evidence for the critical transition to coincide with the cutoff that results in the steepest slope in the strain curve. From this, finite size extrapolation gave a critical cutoff $x_c = 0.616 \pm 0.01$ with a correlation length exponent $\nu = 2$, which is in agreement with the results obtained by means of the order parameter. This is a reproduction of results from the project assignment by Bering (2016), now with better statistics and larger system sizes. With regard to Figure 4.15 in particular it is apparent that better statistics are needed. The estimated x_f for $N = 256^2$ in particular is completely off. Closer examination of the curve indicates that the polynomial fit is not matching the data very accurately near the maximum. However, for the sake of consistency, this point was not adjusted any further. Moreover, this connection was not given high priority, as the critical phase transition of the LLS model not is the main topic of this work.

Notice that the global maximum in the strain curve for the LLS model is reached later than in the ELS model for low cutoff values, i.e. $x_0 \lesssim 0.5$. Thus, one would perhaps expect the LLS model to undergo complete breakdown later in the failure process than the ELS model. In this sense, the LLS model even appear to have a higher degree of global stability in this region.

The strain curve for the LLS model reach ultimate stress at the first fiber that breaks for $x_0 \gtrsim 0.5$, as barely visible in Figure 4.9. Nonetheless the local maxima in the strain curves for the LLS model are reached later than the maxima in the strain curves for the ELS model for $0.5 \lesssim x_0 < 1$. This is seen clearly for $x_0 = 0.617$ and $x_0 = 0.5$ in Figure 4.11 and 4.12 respectively. In this sense the LLS model has a higher degree of local stability than the ELS model for $x < 1$.

However, the strain curve does not tell the complete story. To investigate the global stability of the model, the formerly mentioned stable region ought to be viewed in conjunction with the burst distribution, and the fatal bursts in particular. This topic will first be discussed for the ELS model.

5.4 Burst distribution in the ELS model

As mentioned in Section 2.4, the burst distribution for the ELS model is known to obey a power law $\tau = 5/2$ for large bursts, when the strain curve has a single

parabolic maximum. For the exponential distribution with cutoff, small bursts is known to follow a power law with burst exponent $\tau = 3/2$, with a crossover at Δ_c given by Equation (2.10). This is validated in Figure 4.19. The crossover occurs at the breaking point, when the bundle is undergoing catastrophic failure. With increased cutoff, the unstable region is increasing. For $x_0 = 1$, the strain curve has a maximum for $k = 1$, and is monotonically decreasing, as seen in Figure 2.3. The breaking process is unstable from the beginning, and the power law $\tau = 3/2$ is valid for the entire breakdown process. For cutoffs above 1 the regime with $\tau = 3/2$ narrows, and the burst distribution falls off faster than a power law. This exponential decay is clearly visible in Figure 4.21.

The bursts that cause the entire bundle to rupture is in this thesis denoted as fatal. As pointed out by Kjellstadli (2015), in the ELS model one would expect these bursts to be of size $\Delta_{fatal} \approx N - k_{max}$, where k_{max} is the time step at which the averaged strain curve has a maximum. For the exponential distribution with cutoff, the strain curve of the ELS model has a maximum at $k_{max} = (1 - \frac{1}{e^{1-x_0}})N$. This is in accordance with the results presented in Figure 4.19d.

5.5 Burst distribution in the LLS model

Estimating the burst exponent is not a trivial task. A burst distribution may have different regimes with different burst exponents, or it may not follow a power law at all. On top of this the statistical variations complicate matters even more. Similar to the ELS model, the burst distribution in the LLS model depends on the cutoff in the probability distribution for the thresholds.

The burst distribution with no cutoff is shown in Figure 4.27 for systems of size $N = 64^2$ to $N = 1024^2$. The burst distribution is scaled to fit the power law $D(\Delta) \sim \Delta^\tau$ with burst exponents $\tau = 5/2$ and $\tau = 2.37$ respectively. These figures reveal a behaviour that resembles a power law, however the curvatures suggests a more complicated dependency than a pure power law.

As the cutoff is increased, small bursts occur less frequently and large bursts occur more frequently. This tendency can be seen for $x_0 \lesssim 0.5$ in Figure 4.23-4.24. With a basis in Figure 4.25, the burst distribution in LLS model with $x_0 = 0.6$ appear to be consistent with a power law exponent $\tau = 2$. Figure 4.26 reveal that the fit is better for $x_0 = 0.617$, and even more so for large systems. Moreover, the finite size effects are far more pronounced than for $x_0 = 0$.

Notice the similarities between the LLS burst distribution for $x_0 \in [0.6, 1]$ seen in Figure 4.25 and the burst distribution for the ELS model with $x_0 \in [1.1, 2]$ seen in Figure 4.21. Analog to the behaviour of the burst distribution in the ELS model, the burst distribution in the LLS model is consistent with a power law around the critical state. For higher cutoffs the power law regime narrows, and the burst

distribution falls off exponentially as the cutoff is increased beyond criticality.

On a side note, the fuse model introduced by de Arcangelis *et al.* (1985), is also characterized by a burst exponent $\tau = 2$ near criticality, that is, when the failure thresholds of the fibers are uniformly distributed, cf. Hansen *et al.* (2015). Moreover, this power law character is consistent with the form of the Gutenberg-Richter law of Gutenberg and Richter (1954), which relates the number of earthquakes Ω to the energy release rate by the power law $\Omega \propto E^{-b}$, where b typically is in the range $0.8 - 1.2$, cf. Hansen *et al.* (2015). However, this possible connection is not investigated further.

5.6 Global stability

To relate the bursts to the global stability, it may be useful to study the cumulative probability of a fatal burst occurring during the failure process, $P(\Delta_{fatal})$. How many of the fibers in the bundle may break before the bundle is in imminent danger of catastrophic failure? For the ELS model, Figure 4.20 reveals that the system gradually approaches a critical state as the cutoff is increased from zero to one. Note that the inflection points in $P(\Delta_{fatal})$ coincides with the maxima in the strain curves, as should be expected.

The onset of the fatal bursts in the LLS model is also directly related to the global maximum of the strain curve for $x_0 \lesssim 0.5$. However, closer examination provides evidence for the expectancy values for the onset of fatal bursts to slightly precede the time step at which the maxima occurs in the averaged strain curves. This originates from the high fluctuations in the strain curve before the local maximum, discussed in Section 5.3.

In Section 5.3 it was also pointed out that the global maximum in the strain curve for the LLS model is reached later than in the ELS model for $x_0 \lesssim 0.5$. Closer examination of Figure 4.20 and Figure 4.28 does indeed reveal that more fibers may break in the LLS model than in the ELS model before a fatal burst is to be expected when the cutoff is in this region. In this sense, the LLS model is globally more stable than the ELS model in this region.

The particular cutoff $x_0 = 0.5$ needs to be studied in some more detail. For this cutoff value, the average stress for is highest for the first fiber that breaks. With a basis in this averaged strain curve, one would might expect the onset of fatal bursts to occur either early in the breaking process or perhaps around the local maximum. However, according to Figure 4.28 the bundle is expected to rapture shortly after $k/N = 0.4$, and hence the LLS model is still marginally more globally stable than the ELS model, for which $k_{max} \approx 0.39$. On top of this, the onset of the fatal bursts even appear to coincide with the local minimum in the strain curve for this particular cutoff. This might give the impression of a contradiction, however the

comparison of the averaged strain curve with the strain curve of a single sample in Figure 4.12 provides clarification on this subject. Notice that the maximum value of the single sample is preceding the maximum value of the averaged curve. The fatal bursts represent an average of the extremal values, which follows a completely different distribution than the average of all values.

Kjellstadli (2015) discusses how the LLS model approach the ELS model when the dimensionality increases. In this thesis the averaged strain curves are compared with the strain curve for a single sample for 1-5 dimensions, displaying a reduction of fluctuations with higher dimensionality. This is explained by the fact that the number of nearest neighbours of each fiber increase with the dimensionality, reducing the shielding effect discussed in Section 5.3.

The distribution of fatal bursts in Figure 4.28 reveals a drastic change of behaviour around the critical transition, interpreted as a loss of global stability. For cutoffs above x_c far fewer fibers may break before the bundle is expected to collapse in a force controlled experiment. This sharp transition is not seen in the ELS model, which is no longer globally stable when $x_0 \geq 1$.

The fatal bursts are expected to occur long before the local stability discussed in Section 5.3 are of any significance. The conclusion is that the shielding of weak fibers due to the short-range interaction of the model would not be enough to prevent the system from collapsing in a force controlled experiment.

It is curious that the loss of global stability appear to coincide with the cutoff that results in the highest local stability. Comparison of Figure 4.28 with the simulations of the bundle state indicate that one would expect the bundle to rapture once the failure process has become localized.

One a final note, one should perhaps emphasize that stability could be defined differently. The ELS model will always be able to withstand a load greater or equal to the LLS model before the bundle would collapse completely.

Chapter 6

Conclusion

When the failure thresholds of the fibers are distributed as $P(x) = 1 - e^{-x+x_0}$, the LLS model displays a local stability not seen in the ELS model, in the sense that the strain curve has a positive slope. By investigating the slope of the strain curve for various system sizes, this indicates that the local stability is highest at the localization transition. From this hypothesis, the critical cutoff was estimated to $x_c = 0.616 \pm 0.01$, with a correlation length exponent $\nu = 2$. This is in accordance with the calculations of the order parameter, determining $x_c = 0.6173 \pm 0.0005$ with a critical exponent $\beta/\nu = 1.5 \pm 0.1$.

This local stability originates from the following: When the load of the broken fibers is shared by the nearest intact neighbours, only the strong fibers survive in the perimeter of the cluster. Contrary to the ELS model, where all the fibers experience an increased load as more fibers break, the LLS model thus effectively stresses strong fibers more. Moreover, the LLS model is globally more stable than the ELS model with $x_0 \lesssim 0.5$, in the sense that more fibers may break before the bundle would collapse completely in a force controlled experiment. The distribution of these fatal bursts reveals a drastic loss of global stability around the critical transition. For cutoffs above x_c the local stability of the LLS model also lessens, as the distribution of fiber strength is no longer strong enough to compete with the stress-enhancement due to local load sharing. For $x_0 \gtrsim 2.5$ the local stability vanishes completely.

Loss of global stability is related to a change in behaviour of the bursts. For the LLS model, the burst distribution is shown to be consistent with a power law $D(\Delta) \sim \Delta^{-\tau}$ with burst exponent $\tau = 2.0$ around the critical transition. Analog to the criticality of the ELS model at $x_0 = 1$, lower cutoffs results in higher burst exponents, and cutoffs above x_c give rise to exponential fall off in the burst distribution.

6.1 Further research

This thesis leaves multiple questions unanswered. What is the implications of the local stability? Why does the stability appear to be most pronounced around the localization transition, when the system lose global stability? It would be of great interest to relate this to some physical phenomena.

The LLS model has been investigated with failure thresholds assigned according to the cumulative probability distribution $P(x) = 1 - e^{-x+x_0}$. Could the phenomenas discussed here be general for all probability distributions with cutoffs?

The critical exponent ν needs higher precision. This may be found by calculating the order parameter ψ for a range of cutoff values, and estimating the value for x_0 at the half maximum of the derivative $\frac{\mathrm{d}\psi}{\mathrm{d}x_0}$. By repeating this for a range of system sizes, these values may be extrapolated to infinite lattice size to reveal x_c and ν, similar to the procedure in Figure 4.15.

It is always preferable to have a faster simulation program, and the optimization process is never completed. By replacing the AVL data structures mentioned in Subsection 3.1.2 with `std::set`, the program might speed up. Moreover, this would probably increase the readability of the program considerably.

The burst distribution is probably the quantity that is most readily related to physical experiments, and hence this should be studied in more detail. By investigating the burst distribution in a window of a single sample of large system size, it would perhaps be possible to foresee the fatal bursts by a change in burst exponent prior to the collapse. From this it might be possible to draw some connections to more applied topics, such as forecasting of earthquakes and collapsing mines.

The draft to an article seen in the Appendix demands further development before it is ready for publication. Moreover, an article concerning the localization transition is also in the process of writing.

Bibliography

J. T. Kjellstadli, *Investigating the Local Load Sharing Fibre Bundle Model in Higher Dimensions*, Master's thesis, NTNU (2015).

A. Hansen, P. C. Hemmer, and S. Pradhan, *The Fiber Bundle Model: Modeling Failure in Materials* (Wiley-VCH, Weinheim, 2015).

B. Lawn, *Fracture of Brittle Solids* (Cambridge Univ. Press, Cambridge, 1993).

M. J. Buehler, *Atomistic Modeling of Materials Failure* (Springer, Berlin, 2008).

K. S. Gjerden, *Role of quenched disorder in fracture front propagation*, Ph.D. thesis, NTNU (2013).

S. Sinha, J. T. Kjellstadli, and A. Hansen, Phys. Rev. B **92**, 20401 (2015).

J. Franklin, *The Science of Conjecture: Evidence and Probability before Pascal.* (JHU Press, Baltimore, 2001).

E. Bering, *On the Stability of the Local Load Sharing Fiber Bundle Model*, Project Thesis, NTNU (2016) (unpublished).

M. Dahle, *Critical Behaviour of the Local Load Sharing Fiber Bundle Model*, Master's thesis, NTNU (2016).

S. Pradhan, A. Hansen, and P. C. Hemmer, Phys. Rev. E **74**, 16122 (2006).

A. Petri, G. Paparo, A. Vespignani, A. Alippi, and M. Costantini, Phys. Rev. Lett. **73**, 3423 (1994).

F. T. Peirce, Text. Inst. Trans. **17**, 355 (1926).

A. Stormo, *Brittle to Quasi-Brittle Transitions in the Soft Clamp Fiber Bundle Model*, Ph.D. thesis, NTNU (2013).

D. G. Harlow and S. L. Phoenix, J. Composite Mater **12**, 195 (1978).

P. C. Hemmer and A. Hansen, J. Appl. Phys. **59**, 909 (1992).

L. Onsager, Phys. Rev. **65**, 117 (1944).

D. Stauffer and A. Aharony, *Introduction to Percolation Theory* (Taylor & Francis, London, 1993).

H. E. Stanley, *Introduction to Phase Transitions and Critical Phenomena* (Oxford Univ. Press, Oxford, 1987).

M. E. Fisher and M. N. Barber, Phys. Rev. Lett. **28**, 1516 (1972).

K. Mehlhorn and P. Sanders, *Algorithms and Data Structures. The Basic Toolbox.* (Springer, Berlin, 1999).

T. H. Cormen, C. Stein, R. L. Rivest, and C. E. Leiserson, *Introduction to Algorithms*, 2nd ed. (McGraw-Hill Higher Education, 2001).

M. F. Sykes, M. Glen, and D. S. Gaunt, J. Phys. A **7**, 105 (1974).

C. D. Lorenz and R. M. Ziff, Phys. Rev. E **57**, 230 (1998).

L. de Arcangelis, R. S., and H. Herrmann, Phys. Rev. E **46**, L585 (1985).

B. Gutenberg and C. Richter, *Seismicity of the earth and associated phenomena* (Princeton Univ. Press, N.J., 1954).

Appendix

This appendix contains a draft to an article that will be developed further in collaboration with Magnus H-S Dahle, Jonas T. Kjellstadli, Alex Hansen and Santanu Sinha. The article will be submitted to Physical Review upon completion.

On the stability of the local load sharing fiber bundle model

Eivind Bering,[1,*] Magnus H-S Dahle,[1,†] Jonas T. Kjellstadli,[1,‡] Alex Hansen,[1,§] and Santanu Sinha[2,¶]

[1] *Department of Physics, Norwegian University of Science and Technology, N-7491 Trondheim, Norway*
[2] *CSRC, 10 West Dongbeiwang Rd. Haidan, Beijing 100193, China*

(Dated: June 27, 2016)

We here consider the stability of the local load sharing (LLS) fiber bundle model in two dimensions. When the failure threshold of the fibers are distributed according to $P(x) = 1 - e^{-x+x_0}$, the model display two distinct regimes of behaviour separated by a critical transition. This critical transition is associated with a local stability not seen in the equal load sharing (ELS) model. This stability originates in the short-range interaction of the model, which effectively stresses the strong fibers the most. With $x_0 \lesssim 0.5$ the LLS model is also globally more stable than the ELS model. The LLS model is shown to lose global stability around the critical transition.

PACS numbers: 46.50.+a 62.20.M- 81.40.Np

The fiber bundle models describes systems of N Hookean springs — *fibers* — with spring constant κ and failure thresholds x_i which are placed between two parallel clamps. The form introduced by Peirce 1926 is today known as the *equal load sharing* (ELS) fiber bundle model, and may be described as fibers separated by infinite stiff clamps [1]. When the bundle is extended a length x, the average force per fiber in a strain-controlled experiment will simply be

$$\sigma(x) = x[1 - P(x)] \tag{1}$$

as $N(1-P(x))$ fibers is expected to have a failure threshold above x. With failure thresholds distributed according to

$$P(x) = 1 - e^{-x+x_0}, x \in [x_0, \infty), \tag{2}$$

the *strain curve* $\sigma = \sigma(x = 1)$ may be derived by order statistics [2] to obtain the least force per fiber required to break the next fiber throughout the failure process

$$\sigma = \kappa \left(1 - \frac{k}{N}\right) \left(x_0 - \log\left(1 - \frac{k}{N}\right)\right), \tag{3}$$

where k is the number of broken fibers. The *local load sharing* (LLS) fiber bundle model was introduced as a one dimensional model by Harlow and Phoenix [3, 4]. In this model, the load of the broken fibers is evenly distributed among the nearest intact fibers. Accordingly, the force redistribution rule reads

$$\sigma_i = \kappa\Big[1 + \sum_j \frac{h_j}{s_j}\Big] x \tag{4}$$

where the summation is over all clusters of broken fibers that are nearest neighbour to fiber i. h_j denotes the number of broken fibers in cluster j, and s_j denotes the intact fibers in the perimeter of cluster j, and x is the distance between the clamps if all fibers were intact [2]. This expression is independent of dimensionality. Moreover, this choice of force redistribution is *history independent*, the outcome does not depend on the order in which the fibers have broken.

To determine which fiber will break next, we apply *quasistatic loading*. After a fiber breaks, the extension of the fiber bundle x is reduced to zero, and then increased until another fiber breaks. With this approach only one fiber breaks for each time step. The first fiber to break will be the one that reaches

$$\sigma_i = \kappa x = \kappa x_i \tag{5}$$

first. With the observation $\sigma_i(x = 1) = \sigma(1) = \kappa$, a general breaking rule may be expressed as

$$\max_i \left(\frac{\sigma_i(1)}{x_i}\right) = \frac{\kappa}{x} \tag{6}$$

which is applicable for all the subsequent breaking fibers [2]. For simplicity, we set $\kappa = 1$ in the following.

Where the ELS fiber bundle model is extreme in the sense that it redistributes the force carried by the failed fibers equally among all surviving fibers wherever they are placed, the LLS fiber bundle model is extreme in the opposite sense: only the nearest survivors, pick up the force carried by the failed fibers. There are multiple models that are intermediate between the two extreme models, e.g. the γ model of Hidalgo et al. [5] and the soft clamp model [6–9].

When the failure threshold of the fibers are distributed according to Eq. (2), the LLS model display two distinct regimes of behaviour separated by a critical transition [10]. Systems with low cutoffs resembles the ELS model, whereas systems with high cutoffs are dominated by invasion percolation. These regimes are separated by a critical phase transition known as the the localization transition, described with the order parameter

$$\psi = \left\langle \frac{1}{\max_k\{n(k)\}} \right\rangle \tag{7}$$

where n is the total number of clusters in the system. Localization occur at the critical cutoff $x_0 = x_c = 0.6173 \pm 0.0005$ [11].

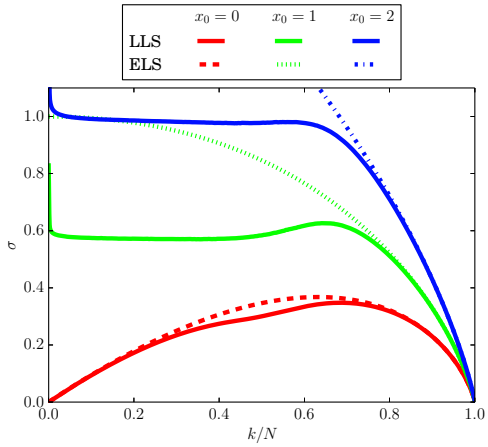

FIG. 1. (Color online) *The strain curve* for the LLS and ELS model for $x_0 = 0, 1$ and 2. The LLS curves originate from systems with size $N = 512^2$ and is averaged over 2^{12} samples, compared with the analytical ELS strain curve.

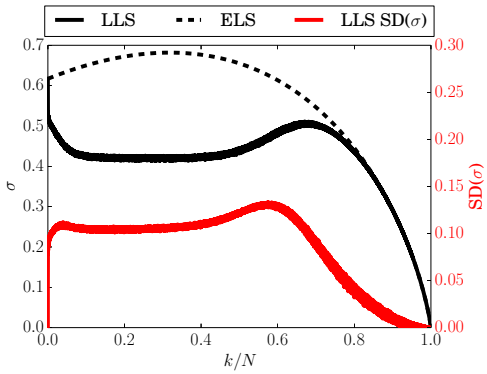

FIG. 2. (Color online) *The strain curve* for the LLS and ELS model for $x_0 = 0.617$. The LLS curves originate from systems with size $N = 512^2$ and is averaged over 2^{13} samples, with standard deviation as red dual axis. This is compared with the analytical ELS strain curves shown as stapled lines.

Sinha, Kjellstadli and Hansen [12, 13] found that the LLS model displays a local stability not seen in the ELS model. Notice that the strain curve for $x_0 = 1$ in Fig. 1 has a positive slope in a region where the strain in the ELS model is decreasing. This gives the impression that in a force controlled experiment, one would have to increase the external load for the breaking process to continue. This stable region vanishes for high cutoffs. By estimating the slope in the strain curve in the region $0.4 < k/N < 0.7$ for $x_0 \in [0, 1]$, Fig. 3 provides evidence for the stability to be highest around the critical transition, and this is more pronounced for larger system sizes. From this hypothesis, the finite size critical cutoffs x_f may be estimated from the maxima of these curves. By calculating x_f for systems of size $N = 64^2$ to $N = 2048$, the critical cutoff was estimated to $x_c = 0.616 \pm 0.01$ by extrapolation to the thermodynamical limit. All maximum values are approximated by second order polynomial fitting.

This local stability originates from the following: When the load of the broken fibers is shared by the nearest intact neighbours, only the strong fibers survive in the perimeter of the cluster. This leave collections of intact fibers encapsulated by walls of fibers with higher failure threshold. When the growing cluster has no new areas to spread to, it is forced to tear down the walls of strong fibers. This expose the collections of intact fibers with lower failure threshold, that typically collapse at once upon interaction with the growing cluster. This process gives rise to high fluctuations, and causes the average external load on the bundle to increase. This also explains the maximum in the curve for the standard deviation of the strain curve seen in Fig. 2. Contrary to the ELS model, where all the fibers experience an increased load as more fibers break, the LLS model thus effectively stresses strong fibers more.

To investigate the global stability of the model, the formerly mentioned stable region may be viewed in conjunction with the cumulative probability of a fatal burst occurring during the failure process, $P(\Delta_{fatal})$. How many of the fibers in the bundle may break before the bundle is in imminent danger of catastrophic failure? For the ELS model, Fig. 5 reveals that the system gradually approaches a critical state as the cutoff is increased from

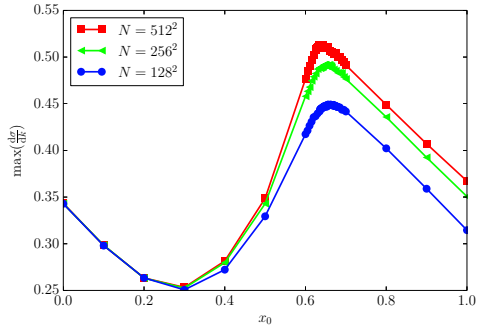

FIG. 3. (Color online) *The maximum slope of the strain curve* for the LLS model is estimated for systems with size $N = 128^2$ to $N = 512^2$ with $x_0 \in [0, 1]$. The data is averaged over $2^{30}/N$ samples, and close to the maxima where the frequency of points is higher, the number of samples is doubled. x_f is estimated at the maxima.

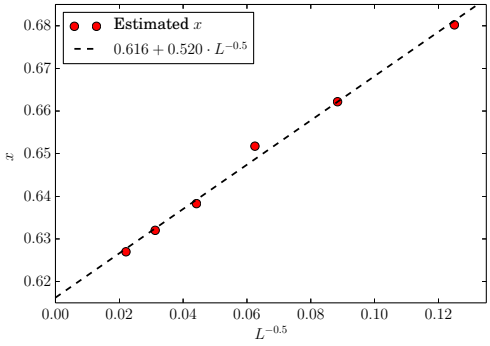

FIG. 4. (Color online) *Extrapolation to the thermodynamical limit* of the finite size critical cutoffs from the systems with the highest positive derivative in the strain curve, for system of size $N = 64^2$ to $N = 2048^2$. The data is averaged over $2^{31}/N$ samples.

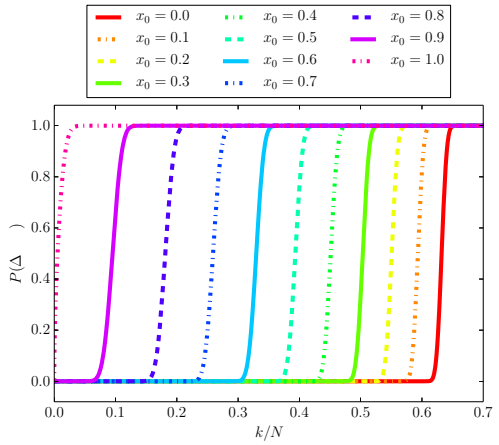

FIG. 5. (Color online) *Fatal bursts for the ELS model* for $x_0 \in [0, 1]$. The systems is averaged over $2 \cdot 10^{16}$ samples.

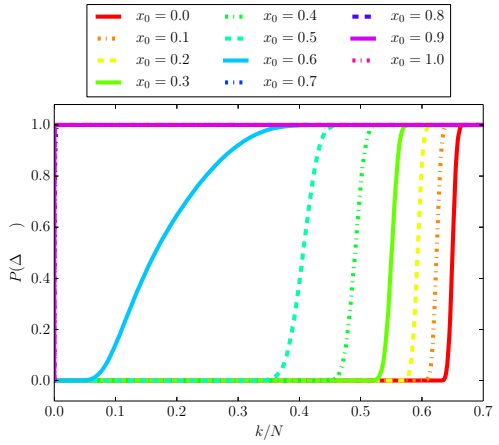

FIG. 6. (Color online) *Fatal bursts for the LLS model* for $x_0 \in [0, 1]$. The systems with $x_0 \in [0, 0.5]$ is averaged over 2^{12} samples, and the systems with $x_0 \in [0.6, 1]$ is averaged over 2^{16} samples.

zero to one. Moreover, the inflection points in $P(\Delta_{fatal})$ coincides with the maxima in the strain curves.

The onset of the fatal bursts in the LLS model is also directly related to the global maximum of the strain curve for $x_0 \lesssim 0.5$. However, closer examination provides evidence for the expectancy values for the onset of fatal bursts to slightly precede the time step at which the maxima occurs in the averaged strain curves. This originates from the high fluctuations in the strain curve before the local maximum. It is important to stress that the fatal bursts represent an average of the extremal values, which follows a completely different distribution than the average of all values.

Ref. [13] discusses how the LLS model approach the ELS model when the dimensionality increases. The averaged strain curved are compared with the strain curve for a single sample for 1-5 dimensions, displaying a reduction of fluctuations with higher dimensionality. This is explained by the fact that the number of nearest neighbours of each fiber increase with the dimensionality, reducing the former mentioned shielding effect.

We thank Håkon T. Nygård and Jørgen Vågan for numerous discussions on this subject, and Morten Vassvik for his great technical assistance.

* eivind.bering@gmail.com
† magnud@stud.ntnu.no
‡ jonastk@stud.ntnu.no
§ alex.hansen@ntnu.no
¶ santanu.sinha@ntnu.no

[1] F. T. Peirce, Text. Inst. Trans. **17**, 355 (1926).
[2] A. Hansen, P. C. Hemmer, and S. Pradhan, *The Fiber Bundle Model: Modeling Failure in Materials* (Wiley-VCH, Weinheim, 2015).
[3] D. G. Harlow and S. L. Phoenix, J. Composite Mater **12**, 195 (1978).
[4] D. G. Harlow and S. L. Phoenix, J. Mech. Phys. Solids **39**, 173 (1991).
[5] F. K. R. C. Hidalgo, Y. Moreno and H. J. Herrmann, Phys. Rev. E **65** (2002).
[6] G. G. Batrouni, A. Hansen, and J. Schmittbuhl, Phys.Rev. E **65**, 036126 (2002).
[7] A. Stormo, K. S. Gjerden, and A. Hansen, Phys. Rev. E **86** (2012).
[8] K. S. Gjerden, A. Stormo, and A. Hansen, Phys. Rev.

Lett. **111** (2013).
[9] K. S. Gjerden, A. Stormo, and A. Hansen, Front. Phys. **2**, 66 (2014).
[10] M. Dahle, *Critical Behaviour of the Local Load Sharing Fiber Bundle Model*, Master's thesis, NTNU (2016).
[11] E. Bering, *On the Stability of the Local Load Sharing Fiber Bundle Model*, Master's thesis, NTNU (2016).
[12] S. Sinha, J. T. Kjellstadli, and A. Hansen, Phys. Rev. B **92**, 20401 (2015).
[13] J. T. Kjellstadli, *Investigating the Local Load Sharing Fibre Bundle Model in Higher Dimensions*, Master's thesis, NTNU (2015).